4 Solar power

4.1 Solar thermal power plants

[A. Neumann]

4.1.1 Overview

The energy conversion in a solar thermal plant starts with collecting the terrestrial sunlight, converting it into heat which is then powering a thermodynamic engine. This engine finally drives a generator which delivers electric energy to the user. The heat conversion path is similar to any other conventional fossil or nuclear power plant. The direct conversion of sunlight into heat using a black flat plate collector leads to temperatures up to 150°C. Designing a power plant with this type of collector and temperature will result in low conversion efficiency (Carnot's law). The solar chimney and solar pond plant schemes are members of this non-concentrating design.

Higher temperatures and better efficiencies are achieved if the sunlight is concentrated before the conversion to heat takes place. There are several optical systems for concentration of sunlight for power production or process heat generation:

- *Dish*
  Three dimensional focusing, direct Sun-tracking paraboloidal mirror, temperatures above 1200°C;
- *Tower*
  Three dimensional focusing, two axis tracking heliostats, temperatures up to 1200°C;
- *Trough*
  Single curvature parabolic mirror, one-axis tracking, temperatures up to 450°C.

These optical designs are ranked according to the achievable temperatures. In the dish and tower concept, the hot side temperatures are limited by the available materials and heat exchanger technology. Basically, the concentrator and heat exchanger can be coupled to the combined gas/steam turbine technology with high efficiency.

The concentrating technologies rely on the availability of direct sunlight, which restricts their application to locations with high irradiance potential mainly in the Sun belt. The discontinuous delivering of energy in case of solar applications suggests the use of an energy storage. The solar thermal power conversion scheme is well adapted to the implementation of a heat storage. This is an advantage compared to technologies that directly produce electricity (wind turbines, photovoltaic cells) because storing heat in large quantities can be done at lower costs compared to direct electric energy storage (e.g. batteries). An efficient usage of a heat storage means that high temperatures should be used. This requirement points into the direction of high concentration dish or tower technologies. On the other hand the solar thermal path offers the possibility of co-firing, i.e. switching on a fossil fuel burner in periods without sunshine.

Several solar thermal power plants have been built up to now. The dish technology has been tested up to 150 kW of electric power per dish, tower plants were operational up to 10 MW. The trough technology is operating in different plants with up to 80 MW per block.

With these solar thermal technologies it will be possible to supply a not negligible fraction of the worldwide consumption of about 15500 TWh (year 2000 status) of electric energy per year. The exploitation of the solar thermal option is mainly restricted to geographical locations with high direct normal irradiance. These regions are located in the Sun belt around the equator, are mostly deserts and have dry climates. But with the rapidly progressing developments in high power transmission technology like DC high voltage conversion and transmission [see LB VIII/3A, Chap. 5: Transmission of electric power] the transport of the energy is possible over thousands of kilometers with only minor losses. This enables the connection of power plants located in high solar irradiance sites to large cities or industrial complexes that are located in mid latitudes or in regions with high population density or urbanization.

4.1.2 Principles of the technology of solar thermal power plants

The following chapters describe different options for the conversion of the solar irradiance reaching the Earth into electricity for human applications. The direct conversion of the solar photons into electricity can be performed by using semiconducting materials in photovoltaic cells. The photovoltaic technology is presented in Sect. 4.2.

The options shown in this section are based on a conversion to electric power by using the thermal path. In this concept the solar light has to heat up a solid, liquid or gaseous medium and the thermal energy is then converted by a thermodynamic process into electricity. The solar thermal option offers the possibility of using power conversion block techniques well known and vastly used in fossil or nuclear power plants. A solar thermal system is suited for the implementation of a thermal energy storage, a necessity for allowing power production during unfavorable sunshine conditions and during night time.

The solar thermal technologies are strongly coupled to the resources of direct solar irradiance and to optical principles for concentrating the radiation reaching the terrestrial surface. Therefore, basics on radiation and related optics are presented first in the next sections.

4.1.2.1 Solar radiation

The Sun is a star with an average temperature of 5777 K of the photosphere, which can be regarded as the "surface" of the Sun. This temperature leads to electromagnetic radiation leaving the solar photosphere with a flux density of $M_{sun} = 63.2 \cdot 10^6$ W/m^2. The spectrum of the solar radiation can be approximated by a blackbody spectrum, but the specific optical properties of the photosphere, chromosphere and corona introduce deviations form a perfect blackbody.

On the way to the Earth, traveling an average distance of $d_{se} = 1.496 \cdot 10^{11}$ m, the flux density is diluted by a factor proportional to the square of this distance. The surface area of the suns photosphere is given by

$$A_s = \pi r_{sun}^2 = 1.521 \cdot 10^{18}\ \mathrm{m}^2 ,$$

with the Sun radius $r_{sun} = 6.96 \cdot 10^8$ m. The total power emitted by the Sun through this surface also passes, assuming no loss processes, the much larger sphere around the Sun and having a radius of the Earth-Sun orbit distance. The flux density at the Earth orbit is then given by

$$E_s = M_{sun} \frac{A_s}{A_e} = M_{sun} \frac{A_s}{\pi d_{se}^2} = 1367\ \mathrm{W/m^2} .$$

E_s is called the solar constant. The attenuation factor $A_s/A_e = 2.165 \cdot 10^{-5}$ or its inverse value of 46200 is the maximum concentration of terrestrial sunlight achievable from the basic thermodynamic laws. The extraterrestrial radiation with the flux E_s has to pass the atmosphere and on its way to ground it is attenuated. This attenuation is caused by absorption, Rayleigh and Mie scattering, and therefore depends on many

atmospherical parameters. Not only the intensity is globally attenuated but also the spectrum is modified depending on atmospheric conditions. The influence of the gas species, aerosol and other scattering contents is complex to model or measure [69Kon].

The movement of the Sun with respect to an observer on the ground is a periodic function and can be described by the astronomical coordinates declination and right ascension, or in a horizontal system by elevation and azimuth. The latter system is more common in solar energy applications. The elevation is zero at sunrise and sunset. When the Sun crosses the meridian it has the highest elevation, which can reach 90° for equinox time and geographical locations within the band of –23.5° to +23.5° of geographical latitude. The crossing of the meridian is called solar noon. For the calculation of the solar coordinates many approximations with different accuracies were given [83Iqb], [91Win].

In the case of a vertical path of sunlight through the atmosphere the light must pass the shortest column of atmospheric gases or gas mass. This refers to an elevation of 90°. For lower elevations the path length is increased. With respect to a vertical path one can define the relative air mass *AM* which is a function of the elevation angle Θ:

$$AM = f(\Theta) .$$

AM is a relative measure and has no units. Assuming a simple planar atmosphere, the relationship is

$$AM = \frac{1}{\sin(\Theta)} .$$

This formula is a good approximation of the curved atmosphere if the elevation is higher than about 20°. The curvature of the Earth and also the refraction becomes important for lower elevation angles and more refined formulas will be necessary [89Kas]. The higher air mass values for low elevation angles not only attenuate the solar irradiance but also lead to a change of spectrum. The shorter wavelengths are more affected by scattering which leads to a shift of the spectrum to longer “red” wavelengths. This spectrum may affect absorption properties of any solar absorber and change the average absorption. Figure 4.1.1 shows model spectra for air masses ranging from air mass zero (*AM*0), without atmosphere, up to *AM*5, which corresponds to a solar elevation of 10 degrees. The radiation transfer model used in Fig. 4.1.1 is LOWTRAN 7 [88Kne].

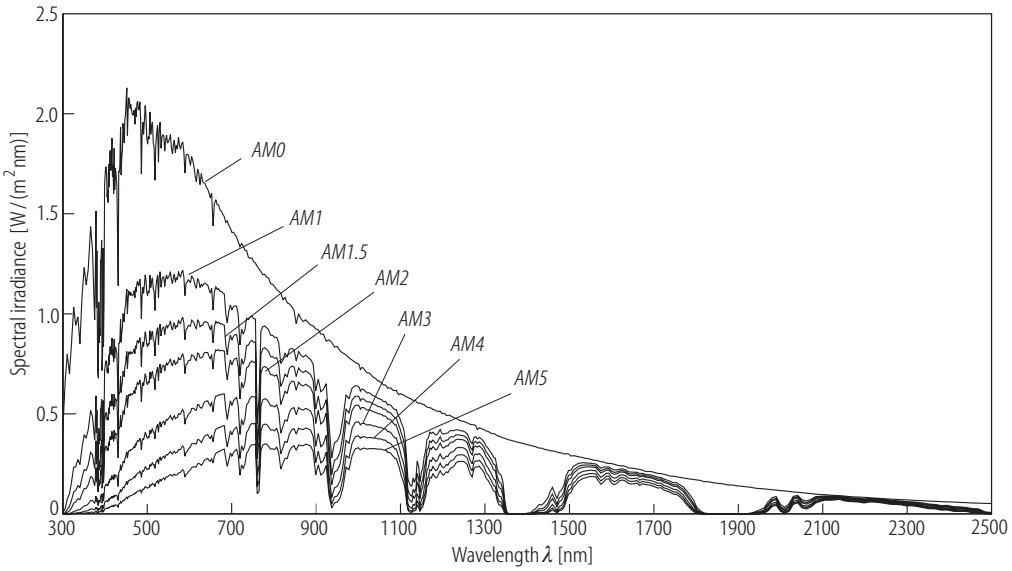

Fig. 4.1.1. Model spectra of the solar irradiance as a function of the air mass *AM*. *AM*0 is the extraterrestrial radiation. The *AM*1 spectrum is the irradiance on the surface of the Earth for a vertical light path.

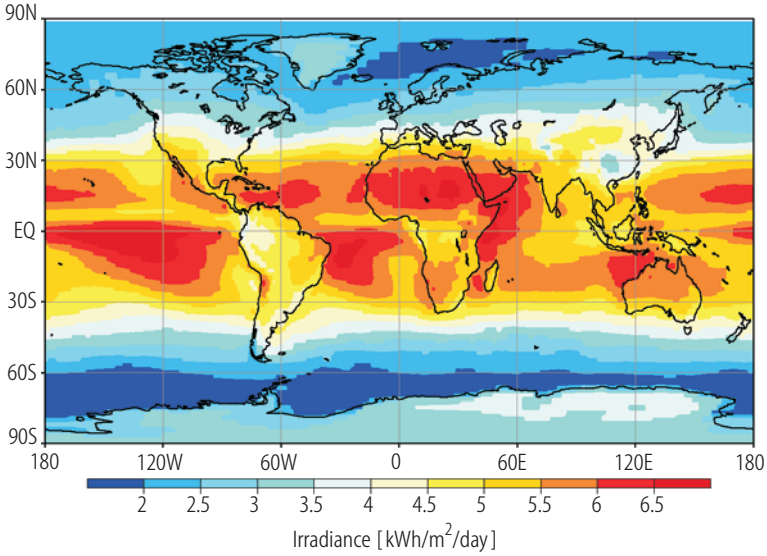

Fig. 4.1.2. Solar global horizontal irradiance map retrieved from satellite data, yearly averages from June 1983 to June 1991. Locations with high solar energy exploitation potential can deliver more than 5 kWh/m² and day on an annual average base. Data source: NASA Goddard Space Flight Center. Data Processing: H. Mächel, Meteorological Institute, University Bonn.

The multiple scattering of solar beam radiation in the atmosphere leads to an attenuation of the direct beam and generates the illumination of the background sky. An observer on the Earth measuring the irradiance on a horizontal surface will record the total or global horizontal radiation E_{tot}, composed of the diffuse scattered radiation E_{diff} coming from the background sky and of the direct normal irradiance E_{dir} sourcing from the solar disk. The direct radiation is defined with respect to a plane normal to the line of sight Earth-Sun and the sine of the elevation must be introduced. Between these irradiances the following relationship holds:

$$E_{tot} = E_{diff} + E_{dir} \cdot \sin(\Theta) .$$

The global radiation is measured with a pyranometer, the diffuse radiation is measured with a pyranometer with a shadow ring for the exclusion of the direct component. A pyrheliometer tracking the Sun is used for recording the direct normal irradiance. It is important to note that a standard pyrheliometer has an acceptance angle of 5° for tracking convenience, which is large compared to the solar disk angle of 0.57°. The average global continuous irradiance on the Earth's surface is about 200 W/m². Locally, on a clear and sunny day, the irradiance can reach or even exceed 1000 W/m², which is about 73% of the solar constant (1367 W/m²).

For designing a solar thermal power plant it is of major importance to have tools for the estimation of the solar irradiance potential on a specific site. As an overview Fig. 4.1.2 shows the daily collectable energy on a yearly averaged basis. This map is retrieved form satellite data and shows that the maximum is about 5-6 kWh/m² per day in favorable locations such as California, Australia, Middle Africa or the Arab countries. As most solar thermal plants are using concentrating technologies the direct normal irradiance is of more importance than the global irradiance because the diffuse component cannot be focused. Table 4.1.1 shows that on a location with good yearly irradiance the energy yield is higher if the direct normal irradiance energy is collected instead of the global horizontal irradiance. At locations with a very modest irradiance, e.g. Cologne in Germany, the global horizontal energy yield is higher than direct normal. Cologne was selected because the meteorological station of the German Aerospace Center DLR Solar Furnace is located there. Concentrating technologies should preferably be used at sites with high direct normal potential.

The daily energy content histograms for several locations are shown in Fig. 4.1.3. The number of available days per year is plotted versus the specific direct normal irradiance (DNI) energy content. Four of the locations listed in Table 4.1.1 are shown. In Cologne most of the days do not contain DNI energy of more than 2 kWh/m². The Dubai test year 1993 shows prevailing daily energy in the 4-6 kWh/m² range. The Daggett data set (years 1980, 1985 and 1990) shows 127 days with 8-10 kWh/m² and even

82 days with 10-12 kWh/m². Only a few days contain less than 2 kWh/m². The yearly variation of the average daily collectable DNI energy is shown in Fig. 4.1.4 for the data sets Daggett, Dubai and Jodhpur. In Dubai in winter time, about 2 kWh/m² per day on an average base are available. On the other hand, the excellent solar site Daggett can deliver up to 10 kWh/m² per day in summer months.

Table 4.1.1. Yearly energy from global horizontal and direct normal irradiance for several locations.

Location	Coordinates	Data source	Global horizontal [kWh/m²]	Direct normal [kWh/m²]
Locations with power plant potential				
Daggett, CA, USA	34.87° N, 116.78° W	1961-1990 RReDC, NREL	2100	2700
Jodhpur, India	26.30° N, 73.02° E	Model Year based on measurements, DLR	2110	2240
Los Angeles, CA, USA	33.93° N, 118.40° W	1961-1990 RReDC, NREL	1790	1750
Glasgow, MT, USA	48.22° N, 106.62° W	1961-1990 RReDC, NREL	1424	1606
Dubai, United Arab Emirates	25.23° N, 55.28° E	Meteo Data 1993	-	1590
Location with poor irradiance				
Cologne, Germany	50.85 N, 7.13 E	1993-1997 DLR Cologne	995	780

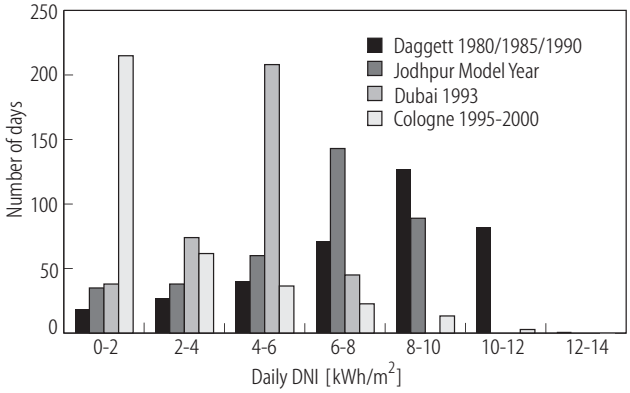

Fig. 4.1.3. Histogram of the number of days available with a specific direct normal irradiance energy content. Four different locations are shown with different solar potential. In Cologne most of the days do not contain noticeable DNI energy. The Dubai test year shows prevailing day energy in the 4-6 kWh/m² range. The Daggett years show 127 days with 8-10 kWh/m² and still 82 days with 10-12 kWh/m².

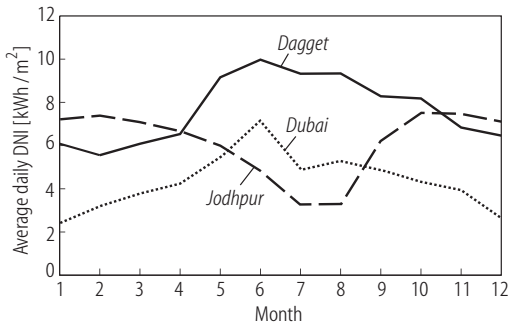

Fig 4.1.4. Yearly variation of the average daily collectable energy for the data sets Daggett, Dubai and Jodhpur.

4.1.2.2 Solar brightness distribution

Concentration of sunlight is often achieved by optical imaging techniques. The well known concepts of image formation with mirrors or lenses apply for these designs, but normally the imaging quality requirements are less restrictive compared to classical optics. The Sun can be regarded as an object at infinite distance with an angular extension cone half angle of 4.65 mrad. In the case of a high concentration imaging system it is of importance to take into account the brightness distribution over the solar disk because this object shape is projected into the image plane (focal plane) of the concentrator [79Big]. The Sun (solar disk) is not a perfect Lambertian light source having a uniform brightness distribution over its surface. The radial temperature profile and the opacity of the solar atmosphere lead to a non uniform brightness distribution over the solar disk [53Kui].

The beam radiation from the extraterrestrial Sun with its darkened limb has to pass the terrestrial atmosphere. The direct beam solar radiation incident on the Earth's surface is not only due to the solar disk with an angular width of about 9.3 mrad but may have, depending on atmospheric conditions, an aureole around the solar disk. In solar energy research, the brightness distribution is often referred to as sunshape. The sunshape is determined by absorption and scattering in the atmosphere. The effect of the forward scattered solar radiation on the sunshape is characterized by the circumsolar ratio (CSR) which describes the ratio of the power contained in the aureole to the total power contained in the solar disk plus aureole:

$$\mathrm{CSR} = \frac{\int_{\text{Aureole}} B(r)\, r\,\mathrm{d}r\,\mathrm{d}\varphi}{\int_{\text{Disk+Aureole}} B(r)\, r\,\mathrm{d}r\,\mathrm{d}\varphi},$$

where $B(r)$ denotes the (rotation-symmetric) distribution of the brightness of the Sun as seen by an observer located at the Earth's surface.

If a solar concentration system based on imaging optics is used, the design of the absorber has to be sized for collecting the image of the solar disk but should take into account the portion of circumsolar light. A design to fit just the solar disk will not intercept all the radiation. As an example, the effect of a variation of CSR on a high concentration solar furnace was shown in [99Neu].

More CSR data for the United States were published in the 1970's by the Lawrence Berkley Laboratories (LBL) [75Gre]. How the sunshape is subject to changes can be seen in Fig. 4.1.5, where several profiles are shown. An extraterrestrial limb darkened Sun [53Kui] is compared to averaged profiles sourcing from measurements. The four profiles display: a very clear day with a CSR of almost 0%, a moderate CSR of about 10%, a high CSR of 20% and an extreme case of 40% CSR. The frequency of occurrence for different CSR conditions is a site-specific phenomenon and requires measurement campaigns. For example, several measurements taken in southern Spain are shown in [98Neu]. The high CSR values of 20% or even more are encountered only in a few percent of all sunshine conditions. Depending on the optical design and the concentration factor, only CSR's higher than 10% will affect the performance of a system. A CSR of less than about 5% is almost negligible for solar energy applications.

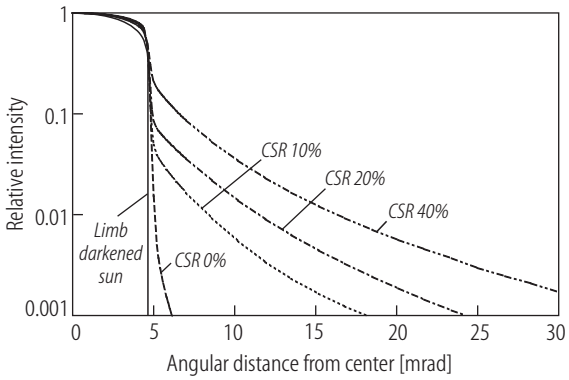

Fig.4.1.5. Profiles of the radial solar brightness distribution. All profiles are scaled to unity at the solar center. The limb darkened sun is taken from [53Kui]; the four CSR curves are averages over measurements from e.g. [99Neu].

4.1.2.3 Optical principles

The solar flux density reaching the Earth surface is still about three orders of magnitude lower compared to power densities in fossil fuel burning flames. This fact leads to the necessity of concentrating the solar light before feeding it into heat and power conversion cycles. In contrast to the optical principles involved in imaging optics designed for high accuracy image formation one has to discuss optical elements of much larger dimensions (e.g. a very rough estimation based on 10 m² collector area for 1 kW_{el} gives a collector aperture of about 1 km² for a 100 MW_{el} plant). The cost factor is much more important than high optical accuracy. The optical properties are only of interest if the beam errors are of the order of the angular extension of the Sun or even larger. The errors due to surface and imaging should be negligible compared to this measure of 10 mrad. This requirement is much less restrictive compared to the precision of a fraction of the wavelength used for imaging optics. For the design of a solar concentrator the basic optical laws of geometrical image formation apply and ray tracing tools may be used for optimizing the layout of a concentrator.

Besides the well known optical imaging systems using lenses or mirrors also radiation concentration based on non-imaging systems found application for solar concentrators. Before discussing optical systems in detail, some preliminary considerations on the limits of concentration are useful.

4.1.2.4 Concentration of radiation

The radiant flux of the direct solar radiation Φ has a flux density E at the Earth's surface. In a loss-free propagation the radiant flux is conserved and cannot be increased:

$$\Phi = \Phi' .$$

Looking at a concentrator according to Fig. 4.1.6, the input flux density E passes through the aperture area A. Conservation of energy yields for the output flux density E' through the exit aperture area A'

$$A \cdot E = A' \cdot E' .$$

Concentration of the flux density, expressed by the concentration factor C, means a reduction in the size of the exit compared to the input aperture:

$$C = \frac{E'}{E} = \frac{A}{A'} .$$

For an ideal concentrator a geometric conservation law for the throughput or etendue is valid [89Wel]:

$$A \cdot \sin^2(\theta) = \text{const} = A' \cdot \sin(\theta') .$$

The square is attributed to the three-dimensional angular concentration for the so-called point focusing concentrators. An angular concentration achieved only in two dimensions (concentration in one plane), keeping one dimension unchanged, leads to a line focusing concentrator which follows the relation

$$A \cdot \sin(\theta) = \text{const} = A' \cdot \sin(\theta') .$$

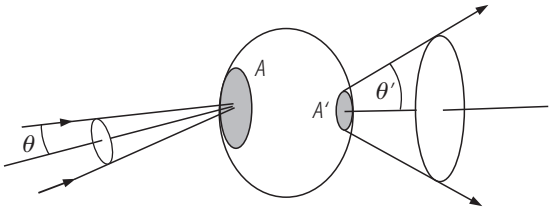

Fig. 4.1.6. Schematic of radiation concentration. The incoming radiation has a beam divergence of θ and is collected over an area A. After concentration the radiation exits through A' with a divergence of θ'.

For a point focusing concentrator, using the above definition for the concentration factor C leads to

$$C = \frac{A}{A'} = \frac{\sin^2(\theta')}{\sin^2(\theta)},$$

which may be extended for ray propagation in media with indices of refraction n and n' to

$$C = \frac{A}{A'} = \frac{n'^2 \sin^2(\theta')}{n^2 \sin^2(\theta)}.$$

By using the Sun half angle of 4.65 mrad, the maximum concentration factor can be calculated. The ray cone at the exit of the concentrator can reach a maximum aperture of $\pi/2$ (= 90°). Thus, the maximum concentration in air (n = 1) is

C_{max} = 46200 for point focusing,
C_{max} = 215 for line focusing.

These concentration relationships are fundamental and not based on any specific design of optical elements like imaging lenses or mirrors. Ordinary imaging systems can not generate exit cones with a ray divergence of up to 90°. The maximum concentration can only be achieved with ideal non-imaging concentrators.

4.1.2.5 Parabolic geometry

The parabolic surface shape is well-known in imaging optics because all the paraxial rays are reflected towards a focal point. Its simple geometry is a good basis for analyzing some of the basic relationships. More details on parabolic geometry and its applications in solar energy can be found in [91Win]. Figure 4.1.7 shows the parameters involved in the parabolic geometry. The relation

$$z = \frac{1}{4 \cdot f} x^2 + b \cdot f$$

holds, where f is the focal length and b the offset parameter in the z coordinate. If b = *-1* the focal point is located at the origin. The angle ψ_{rim} is called the rim angle of the concentrating parabola. Rotating the parabola around the z-axis generates a paraboloidal mirror for three-dimensional focusing. In Fig. 4.1.7, p is the range parameter from a point on the parabola to the focal point. The aperture radius at any point is

$$r = p \cdot \sin\psi,$$

the aperture diameter is $D = 2r$ and the numerical aperture f/D. A parabola with a rim angle of 90° has a numerical aperture of f/D = 0.25.

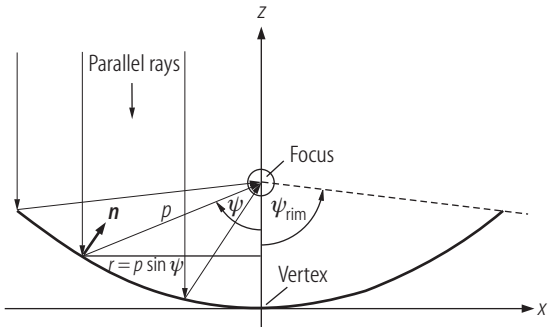

Fig. 4.1.7. Parabolic geometry. Rays parallel to the z axis all cross the focus after reflection. Rotating the parabola around the z axis leads to the paraboloidal concentrator. A line focus is generated if the design is symmetric in the y axis out of the x-z-plane.

Looking at a light source with parallel rays, one sees that all the light is concentrated in the focal spot or line. This is a characteristic feature of a parabola. Figure 4.1.8 shows a more realistic case with a reflection of light ray bundles with a nonzero aperture generated by a distant source (e.g. 4.65 mrad half angle as for the Sun). The bundle falling onto the reflector near to the center line produces a smaller light spot compared to the spot of outer bundles. Increasing the concentration factor by reducing the numerical aperture (larger rim angle) will enlarge the spot size in the focal plane. The contribution of outer bundles to the flux density in the focal point decreases.

There are several options for quantifying the concentration performance. The geometric concentration ratio is defined as

$$C_{\text{geo}} = \frac{\text{Collector aperture area}}{\text{Focal area}}.$$

The focal area is the overall size of the illuminated spot. C_{geo} is ideal in the sense that mirror losses are not taken into consideration. If the flux density is measured at a point *(x,y,z)* in the focus, a local concentration ratio can be defined as

$$C_{\text{loc}}(x, y, z) = \frac{\text{Flux density at point } (x, y, z)}{\text{Direct Irradiance}}.$$

C_{loc} includes mirror losses because it is based on the measurement of irradiances. For example, if the peak flux at a specific point in the focal region of a concentrator is 5 MW/m² and the direct normal irradiance is 800 W/m², the local concentration ratio is 6250. Looking at Fig. 4.1.8 one sees that the intensity in the center, and with it C_{loc}, increases with the rim angle. On the other hand, the light spot area increases too and, approaching 90°, most of the focal plane is illuminated. C_{geo} will have a maximum at a certain rim angle. Figure 4.1.9 shows the geometrical concentration ratio and a loss-free peak flux over the rim angle for a paraboloid. A maximum geometrical concentration of about 11500 is attained for 45°.

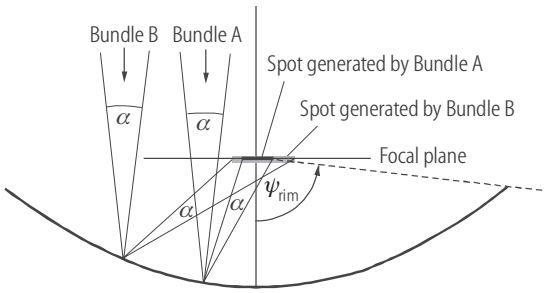

Fig. 4.1.8. Parabolic geometry: Imaging a light source located at infinite distance and occupying a field of view with an aperture α. The image size from the bundle A, close to the axis, gives a smaller spot compared to bundle B.

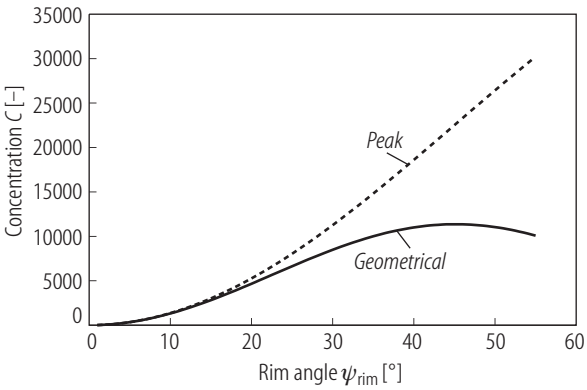

Fig. 4.1.9. Ideal concentration ratio of the paraboloidal mirror.

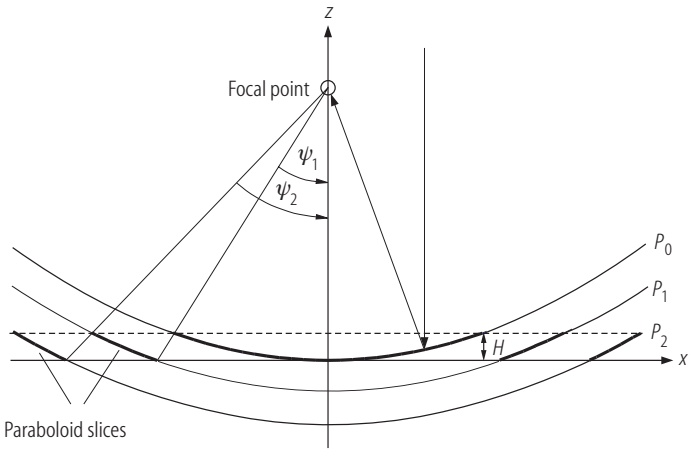

Fig. 4.1.10. Fresnel geometry using three confocal parabolas P_0, P_1 and P_2. The height of the Fresnel optics is H. The curvature of the elements is decreasing with the distance from the central line.

4.1.2.6 Fresnel geometry

Building a large single piece paraboloid is expensive, so other designs would be preferable for the purpose of energy collection. An alternative is the Fresnel reflector which is composed of parabola slices mounted on a flat surface. The flat mounting surface has advantages with regard to practical engineering and construction. The simplest geometry is shown in Fig. 4.1.10. A set of parabolas with a common focal point are superimposed. Three parabolas P_0, P_1 and P_2 are shown, P_0 being the base parabola. The focal lengths obey the equation

$$f_i = f\,\frac{1+\cos(\psi_i)}{2\cos(\psi_i)},$$

where f is the focal length of the base parabola. The outer parabolas have a larger aperture and a smaller curvature. Therefore the curvature is most important for the inner parts. Furthermore, the images of the parabola segments become more and more degraded for the outer parts. The size of the parabola segments is defined by the array's thickness, respectively the height H. The angles ψ_i can be determined as

$$\tan(\psi_i) = \frac{x_{i-1}^{u}}{f-H}.$$

The term x^u is the x-value of the respective parabola for $z = H$. Again, rotation around the z-axis produces a point focusing device, linear extension gives a line focusing array.

The Fresnel geometry principle also found application as a refractive device, the Fresnel lens. The refractive material can be a plastic film and the active surfaces may be manufactured by pressing grooves into this film. This method can produce low-cost optical elements.

4.1.2.7 Non-imaging optics

If the approach of concentrating light using principles of image formation is given up, many different design schemes of non-imaging optics appear. One of them is the compound parabolic concentrator (CPC). A two-dimensional line focusing geometry is shown in Fig. 4.1.11. Two parabolas R and L are joined so that the focal point of the parabola R lies on the end of the parabola L and vice-versa. The axes

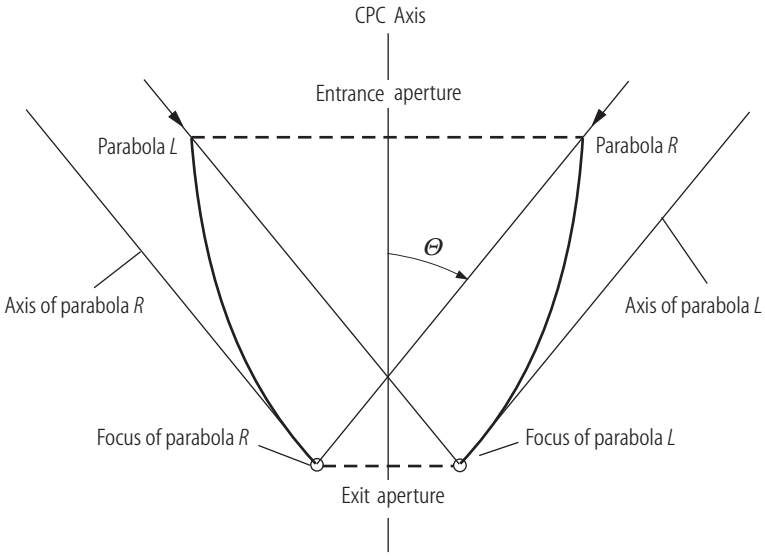

Fig. 4.1.11. Non-imaging compound parabolic concentrator (CPC). All rays entering with angles up to θ exit through the exit aperture, which leads to a concentration of radiation.

of the parabolas are tilted with respect to the main CPC axis by the acceptance angle θ. Rays enteringwith angles $\pm\theta$ are reflected to the respective focal points. All rays entering with smaller angles pass through the exit aperture. Assuming a perfect reflective surface, a uniformly illuminated entrance aperture and a uniform angular distribution of the rays, the two-dimensional CPC is an ideal concentrator with maximum concentration. The concentration ratio is defined by the ratio of the apertures.

Rotation of the parabolas around the main axis leads to a three-dimensional CPC. This device is not an ideal concentrator, even for perfect reflectivity, because skew rays are partly rejected and leave the entrance aperture [89Wel].

Several other non-imaging designs were developed, like the trumpet concentrator, the cone concentrator or truncated designs which will not be discussed here (see [91Win], [89Wel]). Non-imaging concentrators are mostly employed as secondary stages in combination with an imaging primary concentrator.

4.1.3 Designs for concentrating solar radiation

This section contains some of the main designs that have found applications in concentrating solar technology, all based on the principles shown in the previous chapters. Each design would need a detailed optical analysis for deducing performance and flux density distributions in the focal planes or volumes. The references [81Har], [91Win] give more information as well as further literature.

4.1.3.1 Paraboloidal reflector

This is the most simple optical design for the concentration of sunlight, and some of its main features were shown in Sect. 4.1.2.5. This reflector type is called dish and has a curved surface shaped as a rotationally symmetric parabola. For almost parallel light this shape can provide high concentration factors. The reflector must be actuated to follow the path of the Sun (see Fig. 4.1.12) because astigmatic aberrations are prohibitive for somewhat larger misalignment. It can be seen in Fig. 4.1.12 that the sun tracking implements that the focus is not stationary in space and time and is located above ground at a distance of the order of the diameter of the concentrator.

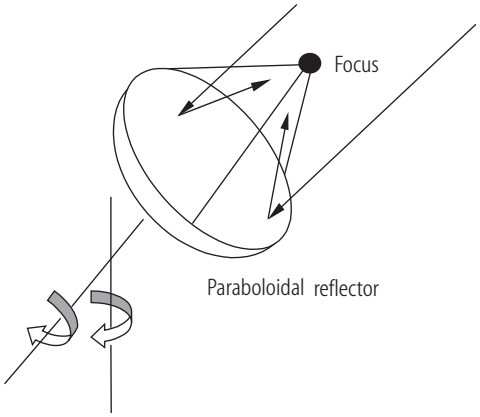

Fig. 4.1.12. Paraboloidal reflector. It is the simplest geometry for concentrating sunlight. The reflector needs a tracking mechanism for following the sun movement across the sky.

4.1.3.2 Spherical reflector

This design is similar to the paraboloidal reflector and well-known in imaging optics (Fig. 4.1.13). The surface has the contour of a sphere segment. A spherical segment with a diameter much smaller than the sphere radius is a first order approximation of a parabola. Manufacturing is simplified because of the spherical symmetry. For energy collection purposes a high concentration factor, which means small *f/D* factors, is more important than high image quality. But for small *f/D* the spherical aberrations are detrimental. In that case the peak concentration factor is not higher than several hundreds. As shown for the paraboloidal reflector, the surface must move in order to follow the path of the Sun.

4.1.3.3 Hemispherical bowl concentrator

In this design, shown in Fig. 4.1.14, a fixed hemispherical reflector is used. The light is focused on a region determined by the caustic of the reflected rays. The absorber has to be moved on a pivot point in the center of the sphere and pointing away from the Sun vector. This design has an upper concentration limit of about 800 [88Wil].

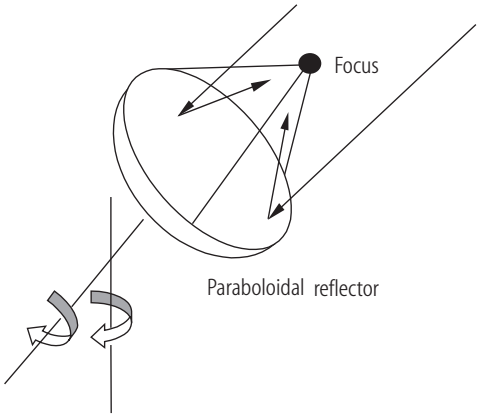

Fig. 4.1.13. Spherical reflector. It is well-known from conventional optics and easier to manufacture than the paraboloidal reflector.

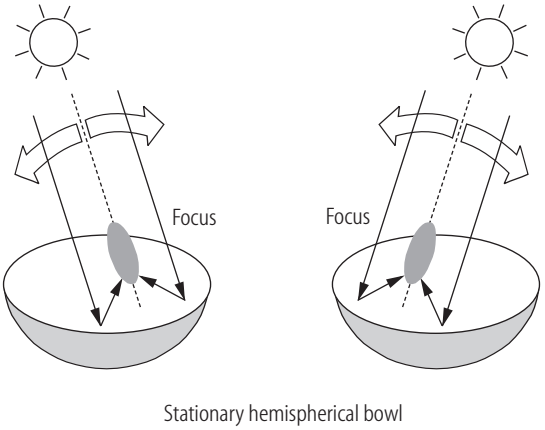

Fig. 4.1.14. Hemispherical bowl concentrator. Its simple geometry is symmetrical with respect to a moving sun. The focal spot quality is poor.

4.1.3.4 Two-stage heliostat concentrator design

In the two-stage heliostat and concentrator design, the focus is stationary in space. The term heliostat is used for a reflector that tracks the Sun and forms a stationary light beam for the exiting rays. As shown in Fig. 4.1.15, the heliostat, equipped with a flat mirror, performs the tracking while a stationary concentrator performs the concentration. The disadvantage in this concept is the second reflection with its associated losses and the higher system complexity. The advantage of a stationary focus is important for absorbers that are position-sensitive or must be kept in a controlled environment. The two-stage design has proven its advantages for experimental facilities like solar furnaces for research purposes. These installations require a fixed focal position and a highly flexible infrastructure around it.

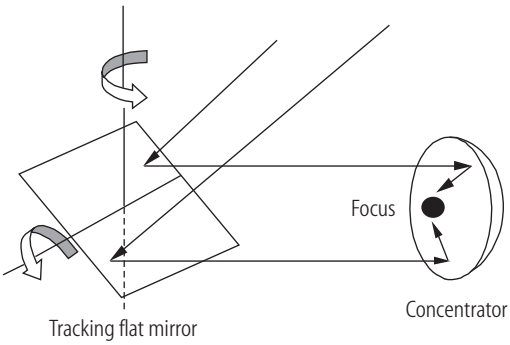

Fig. 4.1.15. Two-stage heliostat and concentrator design. In this layout the focus is stationary in space and the task of tracking is done by a flat heliostat. The light is focused by the concentrator.

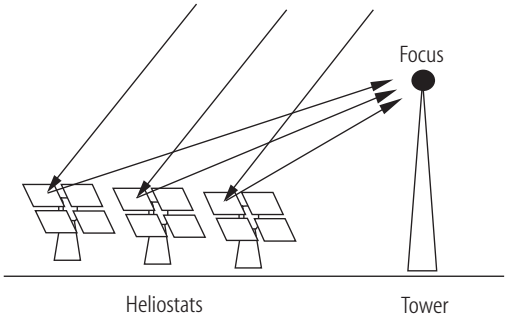

Fig. 4.1.16. Tower concentrator. Tracking concentrating heliostats generate a focus at the top of a tower. This design meets the requirements for large scale systems.

4.1.3.5 Concentrating heliostats and tower

The design using a number of heliostats as shown in Fig. 4.1.16 leads to a stationary focus as well. The heliostats are equipped with concentrating mirrors and reflect the Sun to the top of a tower. The design corresponds to a modified and variable Fresnel optical system. It would also be possible to use small flat mirror heliostats if the mirror surface size is equal or less than the projected solar image at the focal plane. The heliostat and tower concept meets the requirements for large scale systems. Building a tower is a well-known conventional task. The construction of a large number of identical heliostats has potential in cost reduction. A disadvantage is that part of the power plant (receiver, piping) has to be mounted in and on top of the tower.

4.1.3.6 Beam down tower design

The basic design of this beam down approach is based on heliostats and a tower as discussed above. As can be seen in Fig. 4.1.17, a secondary mirror is placed on top of the tower. This mirror reflects the beam down to the ground. The receiver and all the power block systems can be grouped together on ground level, and losses in long pipework are avoided. A drawback is the higher complexity of the optical system.

4.1.3.7 Parabolic trough reflector

The parabolic reflector trough is a design like Fig. 4.1.18 that concentrates onto a focal line. This is the linear extended version of the parabolic geometry discussed in Sect. 4.1.2.5. The maximum concentration factor is 215 and this design is useful only for mid-range temperature applications. The device can have a two axis tracking system, but the main advantage of a linear system is that, if long arrays are used, a single axis tracking gives similar performance compared to a two axis tracking system with significantly reduced complexity.

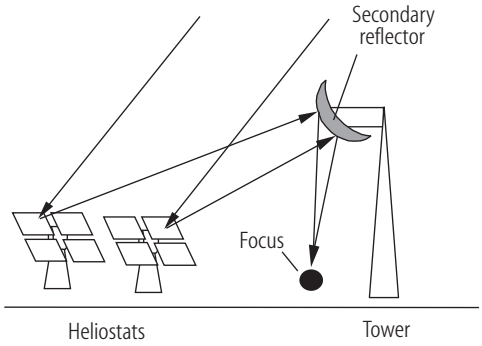

Fig. 4.1.17. Tower beam down concept. A secondary reflector on top of the tower projects the beam down to the ground which makes the access to the receiver and engines easier.

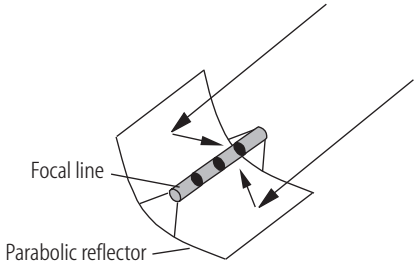

Fig. 4.1.18. Parabolic trough reflector. It has a mirror curved only in one dimension. This device can have a one axis or a two axis tracking system.

4.1.4 Solar to thermal energy conversion

4.1.4.1 General consideration

In a conventional fossil fuel or nuclear power plant, the energy stored in chemical or nuclear form is extracted as primary heat energy in a first conversion. The heat is then converted in a thermodynamic cycle (ideally Carnot, in reality a Rankine, Brayton, Stirling or similar cycle) into mechanical energy which acts on an electric generator. The latter delivers part of the primarily supplied heat energy as electrical power to users.

A solar thermal power plant uses the energy of the sunlight, converts it into heat and then into electricity by means of a thermodynamic process. Therefore, the term solar dynamic energy conversion is sometimes used. The absorber medium is heated by the energy deposited by the sunlight, and part of this heat energy has to be extracted to power the conversion cycle. In terms of fluxes the energy balance is (see Fig. 4.1.19):

$$F_{\mathrm{sol}} + F_{\mathrm{proc}} + F_{\mathrm{amb}} + F_{\mathrm{loss}} = 0 \,,$$

with F_{sol} the solar energy flux, F_{proc} the flux delivered to the process, F_{amb} the flux from the ambient and F_{loss} the loss processes. Regarding the source terms it is assumed that all radiation is completely absorbed (blackbody). Real materials will have absorption coefficients of less than 1 and

$$F_{\mathrm{sol}}^{\mathrm{absorbed}} = \alpha_{\mathrm{sol}} F_{\mathrm{sol}} \,,$$
$$F_{\mathrm{amb}}^{\mathrm{absorbed}} = \alpha_{\mathrm{amb}} F_{\mathrm{amb}} \,,$$

with α_{sol} the absorption coefficient for the solar spectrum and α_{amb} the absorption coefficient for the ambient spectrum. The loss processes are mainly radiation and convection and can be written in a simplified form as

$$F_{\mathrm{loss}} = \varepsilon\sigma T_{\mathrm{absorber}}^4 + \alpha_{\mathrm{hl}}\left(T_{\mathrm{absorber}} - T_{\mathrm{amb}}\right),$$

where ε is the emission coefficient, σ the Stefan-Boltzmann constant and α_{hl} the convective heat transfer coefficient. The convective term, assuming natural convection, becomes negligible for higher temperatures. At absorber temperatures of about 100°C, the radiative and natural convection losses are about equal. At 500°C the convection is of the order of 10% of the loss processes and further diminishes to a few percent at temperatures of more than 1000°C.

The efficiency of the absorption process is defined as flux delivered to the process divided by the incoming solar flux

$$\eta_{\mathrm{absorber}} = \frac{F_{\mathrm{proc}}}{F_{\mathrm{sol}}} \,.$$

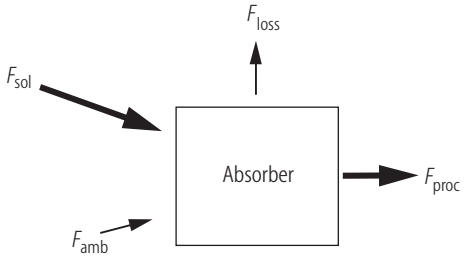

Fig. 4.1.19. Energy balance for an absorber heated by solar light.

Assuming a given concentration factor for the optical design and a given direct normal irradiance, the energy balance can be solved for the absorber temperature and efficiency. Figure 4.1.20 shows the efficiency versus absorber temperature for concentration factors from 1 to 46200. The ambient temperature for the calculation is 300 K, the direct irradiance has the standardized value of 1000 W/m². A natural convective loss term is included with a typical heat transfer coefficient of α = 4 W m^{-2} K^{-1}. The temperature where the curves cross the abscissa, the zero efficiency temperature, is also called stagnation temperature. This is the maximum temperature that the absorber can reach if no heat flux for driving a process is extracted. If heat energy is extracted and used for powering a thermodynamic engine, the Carnot law gives an upper limit to the conversion efficiency of heat to mechanical energy:

$$\eta_{\text{Carnot}} = \frac{T_{\text{hot}} - T_{\text{amb}}}{T_{\text{hot}}} \ .$$

Ideally, without any temperature gradients caused by heat exchangers, the hot reservoir temperature T_{hot} of the Carnot engine is equivalent to the solar absorber temperature and the cold reservoir has the ambient temperature T_{amb}. Assuming an ideal generator with an efficiency of 1 for the conversion of mechanical energy into electricity, the overall cycle efficiency from solar to electric power is

$$\eta = \eta_{\text{Carnot}} \cdot \eta_{\text{absorber}} \ .$$

Figure 4.1.21 displays this combined efficiency of a solar collector coupled to a thermodynamic engine that converts the solar energy to mechanical and electric energy according to the Carnot cycle. An optimum temperature with maximum efficiency is attainable for each concentration factor. A parabolic trough with C = 50 has an optimum temperature of about 400°C, a tower with C = 1000 should operate at about 900°C. The maximum efficiency with the concentration limit of 46200 is 0.84 and the corresponding temperature is about 2320 K (≈ 2050°C). In the literature one sometimes finds 2470 K, which comes from the fact that the extraterrestrial irradiance of 1367 W/m² is used instead of 1000 W/m².

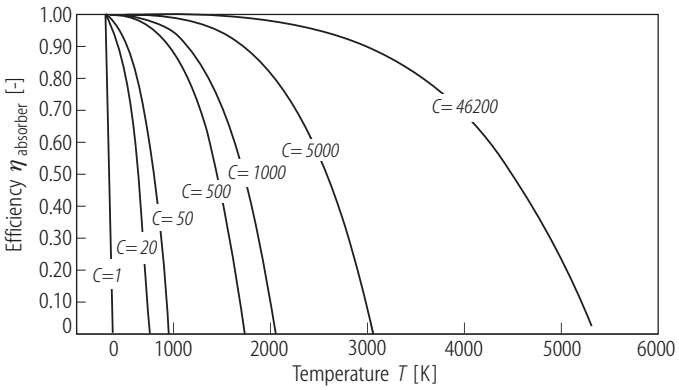

Fig. 4.1.20. Efficiency of a solar absorber for several concentration factors. The temperatures where the curves cross the abscissa are the stagnation temperatures. The ambient temperature is 300 K, the direct irradiance 1000 W/m². A convective loss term of 4 W m^{-2} K^{-1} is included.

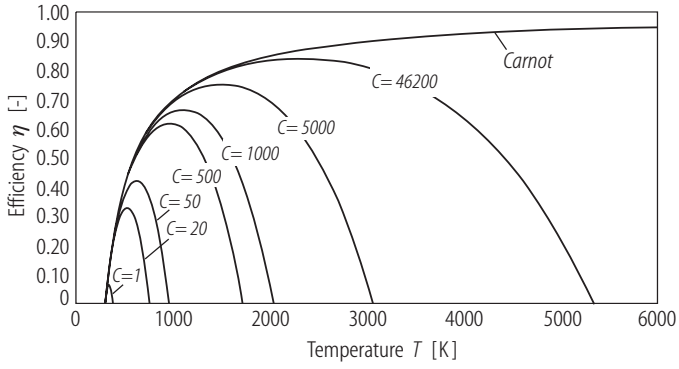

Fig. 4.1.21. Efficiency of a solar collector coupled to a thermodynamic engine that converts the solar energy to mechanical energy according to the Carnot cycle. The calculation was made for an ambient temperature of 300 K, a direct irradiance of 1000 W/m² and a convective loss term.

4.1.4.2 Energy flow in a solar thermal power plant

For analyzing the energy flow in a solar concentrating thermal power plant, Fig. 4.1.22 gives a schematic diagram. The collector is built as an array of concentrating mirrors, represented in the figure by a single mirror, which redirects the light onto the receiver. The latter collects the beam and performs the first conversion. At that point the energy is transferred into the heat transfer medium. The power block contains an engine that transforms the heat into mechanical energy, and a generator performs the last conversion into electricity. For the consideration of the power flow and the loss processes, the following parameters have to be defined (the percentage in brackets refer to the year 2000 state of the art):

P_{in}	Solar radiation intercepted by the collector field;
P_{mir}	Solar radiation scattered and absorbed by the mirrors (1-10%);
P_{air}	Atmospheric absorption of solar radiation from mirror to receiver (0.5-3%);
P_{spi}	Spillage of beam around the absorber (<10%);
P_{ir}	Infrared radiation emitted by the receiver (10-40% of P_{in});
P_{ref}	Light reflected from the non perfect black absorber (<7%);
P_{conv}	Convective losses due to air motion around the receiver (<10%);
P_{cond}	Losses due to thermal conduction into the support structure (<5%);
P_{to}	Concentrated solar radiation reaching the receiver;
P_{rec}	Radiation reaching the receiver aperture;
P_{out}	Usable thermal power output of the receiver;
P_{wh}	Waste heat from thermal to electric conversion (60-90% of P_{in});
P_{el}	Usable electric energy (10-30% of P_{in}).

The overall energy balance can then be written as

$$P_{in} = P_{el} + P_{wh} + P_{ref} + P_{ir} + P_{conv} + P_{spi} + P_{air} + P_{mir} ,$$

while the efficiency of the collector field is

$$\eta_{coll} = \frac{P_{to}}{P_{in}}$$

with $P_{to} = P_{in} - P_{air} - P_{mir}$.

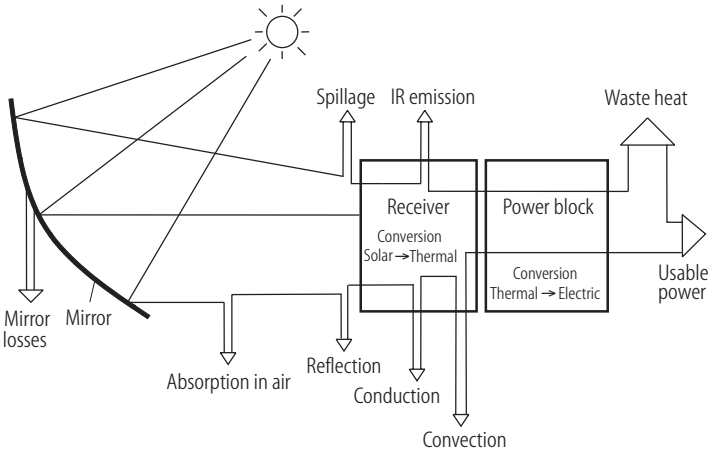

Fig. 4.1.22. Principle of the solar thermal concentration technology. The main components are collecting mirror, receiver and power block.

An important parameter for the characterization of the receiver quality is its conversion efficiency η_{rec} which is defined by the ratio of thermal energy leaving the receiver to the focused solar radiation incident on the surface of the receiver:

$$\eta_{rec} = \frac{P_{out}}{P_{rec}}$$

with the receiver output power $P_{out} = P_{el} + P_{wh} = P_{rec} - P_{ref} - P_{ir} - P_{conv} - P_{cond}$ and the receiver input power $P_{rec} = P_{in} - P_{mir} - P_{air} - P_{spi}$. The receiver is illuminated by P_{to} minus the radiation spilled outside the receiver aperture P_{spi}. The efficiency η_{rec} is of the order of 60-85%.

According to the Stefan-Boltzmann law, the thermal emission P_{ir} of the receiver is proportional to the fourth power of the temperature. Therefore, the surface temperature is of great importance and the receiver design should keep the effective radiation temperature as low as possible.

4.1.4.3 Schematic solar thermal power plant

In a solar power plant, terrestrial sunlight is collected and transformed into heat. This heat is delivered to a thermodynamic conversion engine. The collection and conversion of the terrestrial sunlight (direct and diffuse component) into heat can be done with in a flat plate collector or an isolated greenhouse collector, which leads to temperatures up to 150°C. Designing a power plant with these collectors will result in low efficiencies, as can be seen in the Carnot formula. If no concentration is used, the conversion of solar power into electricity can be performed by direct transformation of thermal energy into kinetic energy of ambient air (wind) by actuating a wind turbine. This is the principle of a solar chimney. In a solar pond, a temperature gradient powers a low temperature Stirling engine or an organic Rankine cycle (ORC).

If in the heat process the involved temperatures are higher than about 100-200°C, the sunlight needs to be concentrated. The optical designs discussed above (i.e. trough, dishes, Fresnel mirrors or towers) can be used for this purpose. By using a parabolic trough concentrator a theoretical maximum concentration factor in air of 215 can be reached. With a three-dimensional focusing, like in the case of dishes or towers, the upper concentration limit is much higher. It is obvious that higher temperatures can be reached in the latter case. The line focus trough system is used up to about 400°C; higher temperatures are possible but would lead to a decreasing absorber efficiency. A tower has the potential of delivering temperatures of more than 1000°C. The direct tracked dish is able to reach even higher temperatures. Here, the upper limit is given by material property limitations. If the sunlight is concentrated to a higher degree in order to generate temperatures of more than 1000°C, engines like a gas turbine or a thermo-ionic converter can be powered. Also, studies were made on the use of magneto-hydrodynamic engines in combination with very high concentrated sunlight.

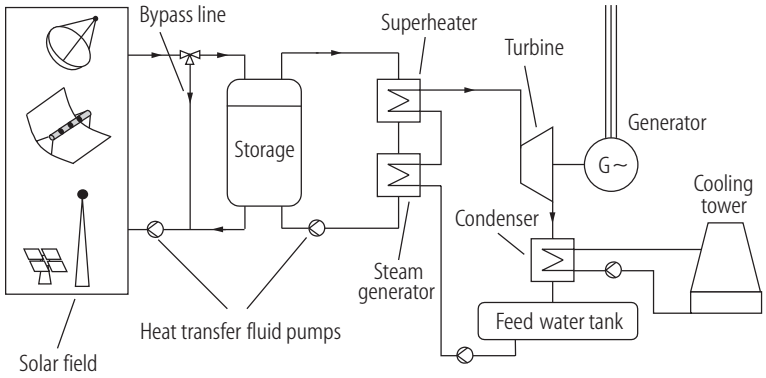

Fig. 4.1.23. Principle of a solar thermal power plant. The solar energy is collected in a heat transfer fluid different from the water/steam loop. The heat transfer fluid passes a steam generator and a superheater. The steam powers a turbine coupled to a generator.

In Fig. 4.1.23, the schematic of a solar concentrating power plant is shown. The first main component is the solar collector/mirror field which collects and concentrates the sunlight. The different designs like dish, trough or tower may be used. The energy is delivered to the heat transfer medium, which is first directed to a steam generator and superheater and finally to the steam turbine. The latter components are basically conventional power plant components.

Common to all solar thermal plants is that a thermal storage can be implemented, which may increase the efficiency of the plant or extend the operation time.

4.1.5 Receiver designs

The receiver is the component that has to convert the sunlight into heat delivered to the transfer medium. It is exposed to harsh environmental conditions (temperature gradients, dust, rain, humidity, frost) because of its outdoors location. The next sections describe some basic designs that were developed for absorbing and converting sunlight. For more and detailed information see [91Win], [91Bec], [95Bec], [93Bec].

4.1.5.1 External receiver

The external or billboard receiver shown schematically in Fig. 4.1.24 is the simplest design that uses high absorption black tubes or plates as radiation absorbers. This design is used in a wide range of applications, from low temperature systems in domestic water heaters up to high temperatures for power plants. The sunlight hits the wall of tubes, and the inside fluid or gas is heated by heat conduction through the wall. The tube walls are exposed to the peak flux density of the beam and therefore have to withstand this load condition. The outside of the tube and its coating reaches the highest temperatures involved. This results in a high power loss by thermal emission. The heat transfer coefficient on the inside of the tubes is important for carrying away the energy and therefore sets limiting conditions to the outside wall temperatures. Figure 4.1.24 shows an example of a multi-tube design with an up and down medium flow. The temperature profile shows that the outside wall temperature must be higher than the heat transfer fluid temperature. The absorption of the concentrated sunlight depends on the absorption coefficient of the wall coating. Black high temperature paint is necessary (absorption coefficients 0.9-0.97). Depending on the quality of this coating, several percent of the input energy is directly reflected by the walls. The largest external receivers were built up to several tens of megawatts of thermal power.

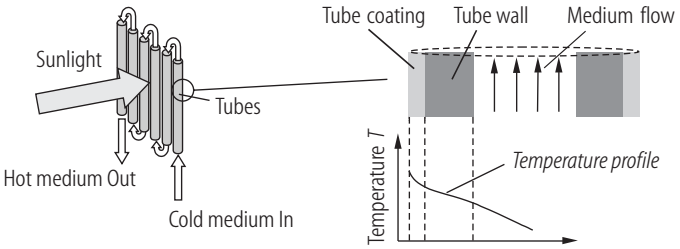

Fig. 4.1.24. Billboard receiver. Absorber tubes or plates are heated and deliver the energy into the heat transfer fluid. The temperature profile (graph at the right) peaks at the outer surface of the tubes.

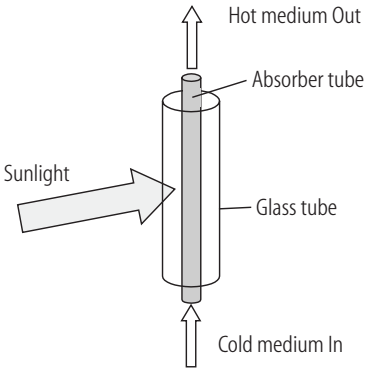

Fig. 4.1.25. Evacuated tube receiver. The absorber tube is separated from the outer transparent glass tube by a vacuum insulation.

4.1.5.2 Evacuated tube receiver

The evacuated tube receiver is a modification of the external receiver. The radiation losses are diminished by putting a glass cover over the absorber walls (see Fig. 4.1.25). The glass is not transparent for long wavelength radiation which is absorbed and heats the glass. Part of this radiation energy is re-emitted onto the absorber wall. A vacuum insulation between absorber and glass further increases the efficiency by eliminating the convective losses. The overall efficiency of this design diminishes for higher temperatures because the thermal spectrum is shifted to shorter wavelengths where glass starts to be transparent.

The evacuated tube receiver has its applications in non-concentrating systems for domestic heating as well as in absorber tubes for parabolic trough collectors in the temperature regime around 400°C.

4.1.5.3 Internal cavity receiver

In the more complex concept shown in Fig. 4.1.26, the heat exchanger is placed inside a cavity illuminated by a beam entering through an aperture. One advantage is the redistribution of sunlight and temperature radiation inside the cavity. This leads to a more uniform radiation distribution on the absorber surface. The point of highest concentration with the highest peak flux in the beam is set in the aperture plane. The radiation flux load on the heat exchanger tubes is lower. The radiative thermal loss is defined by the effective radiation temperature of the cavity. The geometrical effect of a cavity on the absorption coefficient is known from blackbody theory. Even for not very black surface coatings the effective absorption can be increased up to values close to unity.

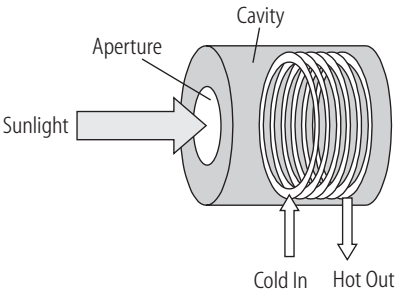

Fig. 4.1.26. Cavity receiver. The absorber tubes (plates) are encapsulated by a cavity.

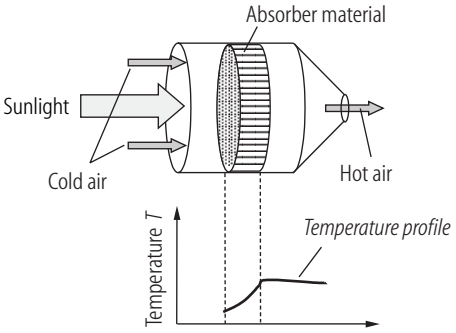

Fig. 4.1.27. Volumetric receiver. The heat transfer fluid flow (air) is parallel to the radiation penetrating the absorber. The temperature profile shows that the colder temperatures face outside; therefore the effective radiation temperature is lower than the maximum air outlet temperature.

4.1.5.4 Volumetric receiver

In this design the energy exchange between light and heat transfer medium occurs in a volume. The direction of the medium flow is chosen in order to have the colder flow facing outside into the ambient air. The effective radiation temperature and the radiative power loss are lower. The sunlight can penetrate into the volumetric absorber region and is able to heat the transfer medium further downstream. This leads to a downstream temperature increase until the maximum exit temperature is reached. Figure 4.1.27 shows a schematic of the volumetric receiver principle and of the temperature profile along the receiver axis. The lower receiver temperature at the entrance causes the main contribution to the thermal radiation emission. This receiver concept has been realized in different modifications. A combined tubular volumetric concept in the 200 kW scale was tested in [91Kes]. Several pressure loaded receivers requiring a window were developed in Germany and Israel [91Win]. The open air volumetric concept directly sucks ambient air into an absorption mesh, a design that needs high volume flow rates because of the low density of the air at ambient conditions. This concept was built and proven up to a scale of 3 MW [94Hae].

4.1.5.5 Direct absorption receiver

The direct absorption receiver is a research concept that is aimed to discard the hot receiver walls that have to transfer the energy. The heat transfer medium is a kind of black gas or fluid in which the energy is directly deposited. There are many problems to be solved in a real application (complex fluid flow, energy exchange problem to ensure a uniform flow and keep other boundary conditions constant in order to reach high efficiencies). The blackness of the gas or fluid may be achieved by doping a gas with high absorptive particles (carbon, silicon carbide, silicon nitride). Figure 4.1.28 shows a schematic of a direct absorption particle receiver. No large scale prototype has yet been built.

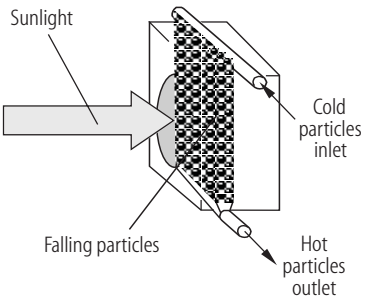

Fig. 4.1.28. Direct absorption receiver. The sunlight directly heats a film of small falling particles which deliver the energy to the flow medium.

4.1.5.6 Comparison of receivers

Table 4.1.2 shows a comparison of a few receiver types that were built for tower plants. The highest heat flux densities were achieved using liquid sodium as heat transfer fluid. The Solar One steam receiver has reached the highest nominal thermal power of 42 MW ever built in a single tower receiver.

Table 4.1.2. Data of several receivers [91Win], [94Hae], [87Sch].

Plant	Receiver type	Peak flux [MW/m^2]	Average flux [MW/m^2]	Power [MW]
IEA-SSPS, Almeria, Spain	Liquid sodium, cavity tube type	1.38	0.35	2.5
IEA-SSPS, Almeria, Spain	Liquid sodium, external tube type, high flux test	2.5	0.35	2.5
Solar One, Barstow, USA	Steam, external tube type	0.6	0.3	42
Themis, Targasonne, France	Molten salt, tube cavity	0.8	0.5	9
TSA, Almeria, Spain	Ambient air volumetric, wire mesh	0.8	0.4	2.5

4.1.6 Storing thermal energy

The solar irradiance illuminating a fixed location on the Earth surface is subject to daily and yearly variations and fluctuations due to cloud coverage. When using this highly variable power source for supplying electric energy to humanity, a mismatch will occur due to the requested power production profile.

Conventional power plants operate as base load plants giving a constant power production over time or as backup plants which deliver the power on demand during high load conditions. Coal fired or nuclear power plants are candidates for base load plants. Gas turbines have a very short startup time and therefore can be used as backup sources. The solar input with its variability will neither fulfill the base load nor the power on demand operation. There are two ways to solve this problem. First, one can implement a power co-production like fossil co-firing in a solar plant. This means that during low solar irradiance periods (cloud transients or at night) a burner supplies the power. This implies that the burner must be able to operate efficiently in any part-load condition between 0-100%, which is a non-standard requirement. The second option is an energy storage system. Adding this type of storage system to a solar power plant is useful for increasing the efficiency of the power generation block because transients and part-load operation may be avoided and it can run more often under nominal conditions.

Storing the energy in form of electrochemical processes in batteries is feasible in small scale systems coupled to photovoltaic collectors. On a larger multi-megawatt scale the use of batteries is prohibitive. Therefore, the energy should be stored as thermal or chemical energy. As a thermal storage is the simplest storage system it will be discussed here in more detail. Chemical energy storage is more appropriate for long-term storage (e.g. hydrogen, see [91Win] or [95Bec]).

An important parameter for the operation of a solar plant with a storage is the capacity factor *CF*. It is defined as the ratio of the annual energy production W_{el} to the theoretically possible yearly energy production capability, the latter being the product of the rated power P_{rate} and the duration of a year (8760 h, 8784 h for a leap year):

$$CF = \frac{W_{el}}{P_{rate} \cdot 8760} .$$

Conventional power plants could in principle reach a *CF* of 100%. But due to periodical maintenance and repair they may run with capacity factors of 80-95%, though. A solar plant without power co-production or storage can only run at a *CF* around 20-35%, depending on nominal power, irradiance conditions and part load efficiency. Introducing an energy storage can increase the *CF* which leads to a collector and receiver design power higher than the plant's rated power in order to fill the storage in periods of high irradiance. This increased solar design power is called solar multiple *SM* and is given by

$$SM = \frac{P_{\text{rec}}}{P_{\text{rate}}},$$

where P_{rec} is the design receiver power and P_{rate} is the design power of the converter.

The capacity of running at nominal power production out of the storage for one hour is called storage hour. As the storage system has its associated losses, the implementation of a storage should increase the power production efficiency by more than the additional storage losses. A storage system as investigated for solar plant application can reach an efficiency of 95% [91Din]; therefore the cycle efficiency has to be raised by more than 5%.

Figure 4.1.29 shows an idealized power time profile of a plant with a storage system. At sunrise t_{sr} the irradiance is too low for operating the plant. From t_{on} on, the plant can operate at rated load P_{rate} and excess power is directed into the storage. This surplus power may go up to the receiver design power P_{rec}. Past t_{off} the solar power is too low for further operation of the solar part but the generator can still operate even after sunset t_{ss} at full load until t_{shut} where the power production has to be terminated. Even without storage it is possible to increase the capacity factor by increasing the solar multiple. This enables an operation of the plant at rated power in irradiance conditions that are below the design point.

The implementation of a storage in the range of 2-3 hours is very useful for increasing the efficiency. On the other hand, a 15 hour storage system will be able to lift the capacity factor to more than 80%. One major focus in plant development is therefore the search for low-cost storage systems and heliostat fields.

Another important aspect concerning the implementation of a storage is the possibility in shifting the peak power production into a time window with high tariffs. If the user energy consumption peaks in the afternoon or evening and not at solar noon it is economically preferable to have enough energy reserves for dispatching power during this afternoon period.

The thermal energy can be stored either in form of sensible heat or as latent heat, using phase transitions. Figure 4.1.30 shows different storage concepts, and in Table 4.1.3 one finds the characteristics of several materials that are dedicated as heat storage media. When designing a heat energy storage, a simple way would be to use the heat transfer fluid directly as storage medium and fill it in a tank. This concept requires a thermal stratification and can only be used with fluids with low heat conductivity (water, oil, see Fig. 4.1.30a). If the physical properties of the transfer medium inhibit a stratification, a dual tank concept is a better option. A hot tank is filled by the solar heated medium and can in parallel provide hot transfer fluid for the power conversion engine. The latter delivers the cold fluid into the cold tank which then serves as source for the solar heating process (see Fig. 4.1.30b). If the heat transfer fluid is expensive, the energy should be stored in a solid and less expensive material. This leads to the dual medium storage design (Fig. 4.1.30c,d). Looking at the material data in Table 4.1.3, an example for the dual medium storage would be a silicone oil or a special molten salt as heat transfer medium combined with a rock or concrete solid as storage material.

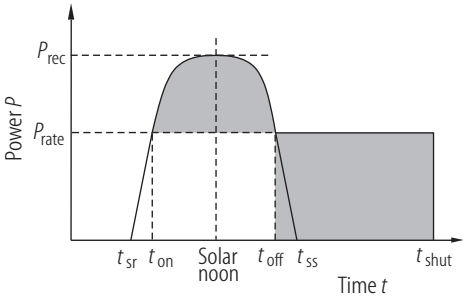

Fig. 4.1.29. Power delivery curve of a solar plant with a thermal storage system. The operation continues after sunset t_{ss} by unloading the storage.

A further major economic issue is that the medium in any storage vessel must be kept at the lowest possible pressure even at high temperatures. The large storage reservoirs have to withstand these pressures. Large vessels under high pressure have important safety issues and cause very high costs. Using water at several hundreds degrees Celsius would require a pressure of 100 bars or even more. Instead of using water, Table 4.1.3 shows some alternatives, e.g. salts that can be used in a molten phase as heat transfer fluid. Molten salts require basically no pressurized vessels. Another solution would be the dual medium tank with tubular heat exchangers as seen in Fig. 4.1.30d, where the energy is stored in a material different from the heat transfer fluid, while the fluid is enclosed in tubes at high pressure.

Table 4.1.3. Media for sensible heat thermal storage application [91Din], [91Win].

Storage medium	Phase	Max temp. [°C]	Density [kg/m^3]	Heat capacity [kJ/kgK]	Volume specific heat [kWh/m^{3}K]	Heat conductivity [W/(mK)]	Approx. cost [$/kg]
Concrete	solid	400	2200	0.85	0.52	1.5	0.07
Sand	solid	1000	1500	0.7-1.2	0.29-0.5	0.6	0.04
Magnesia fire bricks	solid	1600	3000	1.15	0.96	3	2.4
Silica fire bricks	solid	1200	1820	1	0.51	1.5	1.2
Sodium chloride	solid	500	2160	0.85	0.51	7	0.1
Steel	solid	800	7800	0.6	1.3	40-50	0.9
Carbonate salts	liquid	850	2100	1.8	1.05	2	2.5
Liquid sodium	liquid	530	850	1.25	0.295	70	2.0
Mineral oil	liquid	300	770	2.6	0.56	0.12	0.4
Nitrate salts	liquid	560	1870	1.6	0.83	0.52	0.6
Synthetic oil	liquid	390	900	2.6	0.65	0.11	3.2
Water	liquid	95	1000	4.2	1.1	0.6	0.02

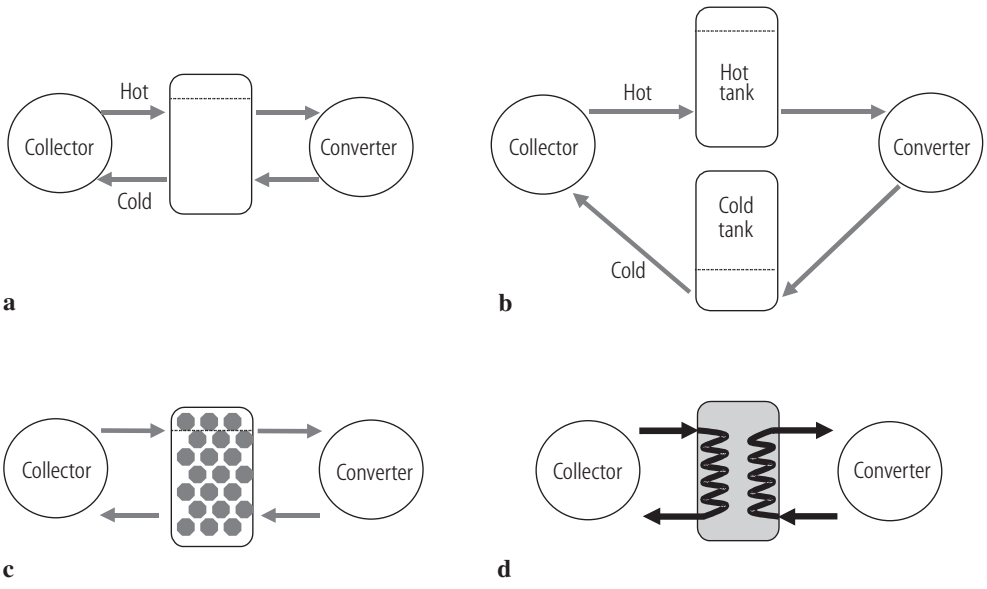

Fig. 4.1.30. Different designs for thermal energy storage. **(a)** Single medium, one tank, thermocline. **(b)** Single medium, dual tank. **(c)** Dual medium, one tank, thermocline. **(d)** Dual medium, one tank, tubular heat exchanger.

Table 4.1.4. Media for phase change thermal storage application [91Din], [91Win].

Medium	Phase change temperature [°C]	Density [kg/m^3]	Melting heat [kJ/kg]	Heat conductivity [W/(mK)]	Cost [$/kg]
K_2CO_3	891	2290	200	2	0.7
Na_2CO_3	851	2533	280	2	0.2
NaCl	802	2160	520	2	0.1
KNO_3	333	2110	116	0.5	0.2-0.8
$NaNO_3$	308	2257	180	0.5	0.2-0.7

A rather new process based on the dual medium concept is to use sand/air as heat transfer fluid and storage material. The design would be similar to Fig. 4.1.30b, and the fluidized sand/air mixture is the working medium. Details of such a system can be found in [03Hof]. Table 4.1.3 shows that the media costs are quite competitive.

Another option is to store the energy as latent energy (liquid phase) and release it by a phase transition liquid to solid. Table 4.1.4 shows several candidate salts. The storage volume or mass needed for a certain amount of energy is much reduced in case of phase change processes. On the other hand, this technology has more issues and the costs are higher. The dual medium concept is best suited for the phase change energy storage process. A fluid serves as heat transfer fluid, and the storage medium is in solid or liquid status, depending on the load level.

4.1.7 Solar thermal power plants

This section will discuss solar thermal projects that were realized and gave operational experience. Survey information about the projects is presented in [95Bec], [91Win], [94Sol].

The schematic diagram of a plant shown in Fig. 4.1.23 is valid for solar technologies where the collector is composed of concentrating optical elements like troughs, dishes or heliostats plus tower. A storage system may be implemented, and the energy finally drives a conventional superheated steam circuit and a turbine. A high concentration technology also has the potential of reaching temperatures of more than 1200°C and therefore to power a gas turbine before feeding its waste heat into the bottoming steam cycle. This combined cycle scheme is able to reach high efficiencies (>50%).

The concept shown in Fig. 4.1.23 could also be extended to the solar pond principle discussed in the next section. There, the collector is a pond and a liquid with a lower boiling point must be used instead of water/steam for powering a turbine.

4.1.7.1 Solar pond power plant

In a solar pond the solar energy is absorbed and stored in a water reservoir. Water is a transparent fluid and sunlight can penetrate layers that are several meters deep. The use of a water pool for storing thermal energy has the major disadvantage that convection brings the hot water to the pool top where the stored energy dissipates easily due to evaporation and convective cooling of the wind. Dissolving salt in the water and giving the salt a vertical gradient of the order of 150 kg/m³/m can inhibit the convective flow. With this stratification it is possible to achieve a temperature profile starting with 30°C at the top to 80-90°C at the pond bottom. Instead of using a salt gradient, a transparent cover (e.g. films, viscous oils) can be used in order to reduce the heat losses from the pond surface.

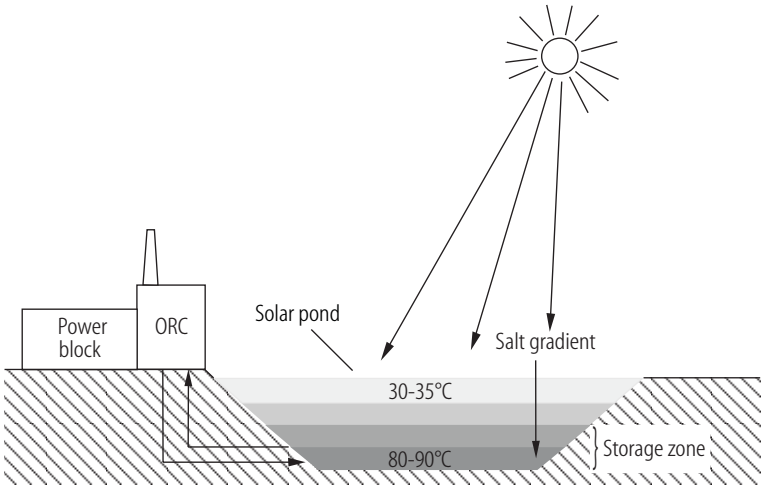

Fig. 4.1.31. Schematic of a solar pond power plant. The salt gradient inhibits convective heat exchange and the warm bottom layer is stable. An organic Rankine cycle engine (ORC) converts the heat into electricity.

Table 4.1.5. Solar pond projects.

Location	Operation	Rated output	Pond surface area [m^2]
Beit Ha' Arava, Israel	1984-/	5 MW_{el}	250000
Alice Springs, Australia	1985-1989	15 kW_{el}	1600
El Paso, USA	1986-/	70 kW_{el}, 300 kW_{th}	3350

Figure 4.1.31 shows the principle of operation of a solar pond. The temperature difference between the bottom of the pond and the ambient temperature is used to drive a low temperature organic Rankine cycle [94Sol]. A modified Rankine cycle using an ammonia/water mixture was also proposed by Kalina [92Kal]. The cycle efficiency of these low temperature engines is of the order of 5-10%, and the overall annual solar to electric conversion efficiency for a test plant in Israel is about 0.9%. In Table 4.1.5, three solar pond projects are listed [94Sol].

The advantages of the solar pond technique are that no glass or mirror surfaces are needed and that the mass of the water in the pond acts as a heat storage system. On the other hand the water quality management and the salt gradient control are major issues.

4.1.7.2 Solar chimney power plant

The solar chimney power plant is based on the idea of heating air inside a greenhouse and letting the hot air escape through a vertical chimney [00Sch]. An entrance aperture in the greenhouse provides a continuous air inflow. The greenhouse acts as a solar collector and its area determines the collectable power. In Fig. 4.1.32, a schematic of a chimney power plant is shown. The collector has a cover made of a transparent material like glass or plastic foil. The soil is heated by the sunlight and the energy is transmitted to the air flowing over it. The air is sucked into the chimney where it is accelerated. The flow at the lower end of the chimney drives a wind turbine and a coupled generator. Inside the chimney the air is undergoing a cooling process by adiabatic expansion.

The solar chimney plant capacity factor is not strictly coupled to direct sunshine. As the ground acts as a thermal storage, the plant can produce power even after sunset or during cloud transients. The capacity factor can be increased by putting a storage material on the ground inside the collector in order to further expand the operation time.

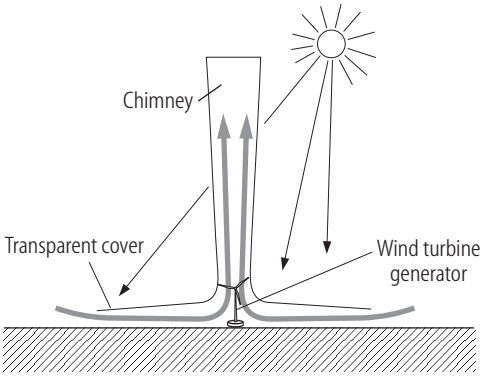

Fig. 4.1.32. Principle of a solar thermal chimney power plant. The sun heats the air under a transparent cover. The hot air is accelerated in a chimney and drives a wind turbine.

Table 4.1.6. Solar chimney power plant project.

Manufacturer	SBP Schlaich, Bergermann und Partner, Stuttgart, Germany
Location	Manzanares, Spain
Rated power	50 kW
Chimney	Height: 194.6 m, Radius: 5.08 m
Mean collector radius	122 m
Mean collector roof height	1.85 m
Heating in collector ΔT	20°C
Wind turbine blades	4 Blades, 5m long
Annual solar to electric efficiency	0.53%
Operation	1986-1989

The efficiency of a solar chimney, defined here as the electrical output divided by the global horizontal irradiance times the covered collector area, is low compared to most of the other solar energy technologies. On the other hand the investment costs may be low because the chimney technology is simple and the plant may be built by local craftsmen. This argument is based on the assumption that land is very cheap because the collector has to be large enough for collecting the nominal power due to the low efficiency. Other advantages of the chimney plant concept are that no water for cooling is needed and that the technology is simple and reliable with only a few moving parts. As with flat plate collectors direct and also diffuse radiation can contribute to the heating process.

A prototype plant was built by the German company Schlaich, Bergermann und Partner in Spain [00Sch]. In Table 4.1.6 the specifications of this plant are listed. The annual solar to electric efficiency was about 0.5%. The efficiency increases with the chimney height and the quality of the collector cover material. Calculations show that 1-5% efficiency may be achieved for chimneys with heights of 1000-1500 m and diameters in the range of 100-200 m [00Sch]. The plant's nominal power for such a design is claimed to be about 200 MW electric.

4.1.7.3 Parabolic trough power plant

The parabolic trough design is a line focusing concentrator that has the advantage to work with a one-axis tracking system. This increases the simplicity of the system and can counterbalance the low temperature and efficiencies achievable with this two-dimensional concentration. For this reason nine major operational solar thermal power plants have been equipped with trough collectors until today.

In Fig. 4.1.33 the schematic of a trough power plant is displayed. The collector field concentrates the sunlight onto absorber tubes located in the focal line. The absorber tubes' design is based on the evacuated glass tube concept. The metal absorber tubes have a selective coating that maximizes the absorption

of sunlight and minimizes the thermal emission. In these tubes the transfer medium can be heated to temperatures of more than 400°C, depending on the optical quality of the collector and on the material properties of the heat transfer fluid. A thermal energy storage system may be implemented for damping sunlight fluctuations or shifting the power delivery curves to match the needs of the users. The thermal storage for the trough technology has to face the problem that the absorber temperature potential is not high and any heat exchanger or storage load/unload will further reduce the temperatures and efficiency.

Table 4.1.7 shows the data of several major trough projects. The SSPS project compared different technologies, for instance two-axis tracking collectors (MAN, Germany) and single axis tracking collectors (Acurex, USA). It turned out that a two-axis system had no net advantage because the movement in two directions with the absence of the cosine loss effect causes higher piping losses and needs a higher number of flexible joints. The single axis collectors needed less maintenance and had a higher average availability. The LUZ company from Israel built the SEGS (acronym for Solar Electric Generating Systems) trough plants in California, USA. The SEGS plants are still operational in 2002 and produce about 0.2 GWh per year. A photograph of a single SEGS trough collector is shown in Fig. 4.1.34. The trough plant at Kramer Junction in California, shown in Fig. 4.1.35, has a nominal output of 150 MW_{el}. The plant is composed of 5 trough arrays and 5 power blocks of 30 MW_{el} each.

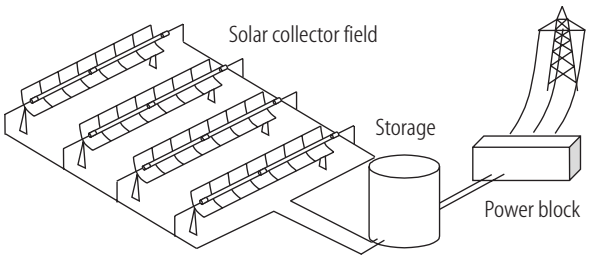

Fig. 4.1.33. Solar thermal trough power plant. An array of trough collectors heats a fluid which is pumped to a power block or can be stored in an energy storage tank.

Fig. 4.1.34. View of a SEGS trough collector at Kramer Junction (source: Kramer Junction Operation Company KJC).

Fig 4.1.35. 150 MW SEGS trough power plant at Kramer Junction (source: Sandia National Laboratories).

Table 4.1.7. Solar parabolic trough power plants.

Name	Location	Operation	Electric output [MW]	Heat transfer fluid, field operating temperature	Storage	Collector field aperture, tracking method
SSPS DCS	Almeria, Spain	1981-1986	0.5	Mineral oil 295°C	Oil, 5 MWht Oil/Cast iron, 4 MWht	4940 m², two axis tracking 2674 m², single axis tracking
SEGS I	Barstow, CA, USA	1985	14	Synthetic oil 307°C	119 MWht	82960 m², single axis tracking
SEGS II	Barstow, CA, USA	1986	30	Synthetic oil 315°C	no	165376 m², single axis tracking
SEGS III	Kramer Junction, CA, USA	1987	30	Synthetic oil 349°C	no	230300 m², single axis tracking
SEGS IV	Kramer Junction, CA, USA	1987	30	Synthetic oil 349°C	no	230300 m², single axis tracking
SEGS V	Kramer Junction, CA, USA	1988	30	Synthetic oil 349°C	no	250560 m², single axis tracking
SEGS VI	Kramer Junction, CA, USA	1988	30	Synthetic oil 390°C	no	188000 m², single axis tracking
SEGS VII	Kramer Junction, CA, USA	1989	30	Synthetic oil 390°C	no	194280 m², single axis tracking
SEGS VIII	Harper Lake, CA, USA	1990	80	Synthetic oil 390°C	no	464340 m², single axis tracking
SEGS IX	Harper Lake, CA, USA	1991	80	Synthetic oil 390°C	no	483960 m², single axis tracking

4.1.7.4 Dish power plant

A paraboloidal mirror that is kept pointing at the Sun by a tracking system is called a dish (Fig. 4.1.36). Using a short focal length, a high quality surface and a high reflectivity it is possible to reach very high radiation concentration and high temperatures. The applications for dishes as part of solar power systems start at small scale single units for remote use but may also range up to plants composed of many dishes, called dish farms.

A great variety of collector and converter unit designs were proposed and realized. With its high temperature potential dishes are suited for high efficient conversion processes like Stirling engines or thermionic converters. Table 4.1.8 lists a few of the dish projects where the conversion to electricity is done via a Stirling engine. Figure 4.1.37 shows the dish Stirling system built by McDonnell Douglas. This dish has a collector made of curved rectangular glass mirrors on a metal support structure. For this system, solar to electric conversion efficiencies of up to 30% were reported [87Joh].

A different collector technology, called stretched membrane technology, is shown in Fig. 4.1.38, the Schlaich, Bergermann and Partner (SBP) dish. The concentrating collector shape is generated by depressurizing a drum closed by two thin stretched metal foils. Thin glass mirrors (1 mm thick) are glued onto the front metal membrane foil. A very similar technique was developed by SBP and the German Steinmueller Company for heliostats for tower plants. The depressurized membrane technique enables the setting of different focal lengths only by adjusting the vacuum inside the drum.

The Australian National University built a large 400 m² dish and implemented a piston steam engine powering a generator [94Sol].

In several projects single dishes were grouped together in dish farms. In these concepts the medium that is heated in every dish is collected in a main line and fed into a central power block [91Kan]. This larger conversion unit can work with better efficiencies compared to a sum of smaller units. Table 4.1.9 shows dish farm projects that operate with Rankine engines (water/steam or organic fluids). The collected energy in the Shenandoah and Sulaibyah plants was, beside electricity generation, used as process heat for drying and cooling applications [88Ney]. Figure 4.1.39 shows an aerial view of the Shenandoah dish farm with its 114 dishes.

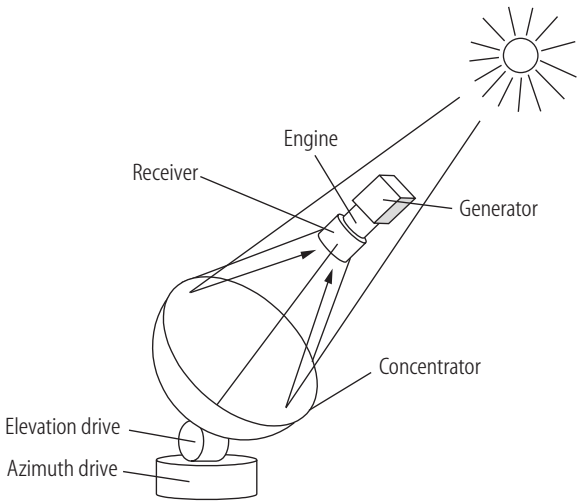

Fig. 4.1.36. Principle of a solar thermal single dish generator. The engine is mounted in the focal plane and the dish has to follow the course of the sun.

Fig. 4.1.37. Dish Stirling built by McDonnell Douglas. The collector is built of glass mirrors (source: Sandia National Laboratories).

Fig. 4.1.38. Dish Stirling built by Schlaich, Bergermann and Partner (SBP). The collector is built as a stretched membrane coated with thin glass mirrors. The sunlight powers a Stirling engine (source: SBP).

Fig. 4.1.39. View of the dish farm at the Shenandoah Solar Total Energy Project, GA, USA (source: Sandia National Laboratories).

Table 4.1.8. Dish Stirling projects.

	Vanguard, USA	McDonnell Douglas, USA	SBP, Germany	SBP, Germany	Cummins Power Generation, USA	SAIC, STM, USA
Location	Rancho Mirage, CA, USA	Los Angeles, CA, USA	Riyadh, Saudi Arabia	Almeria,Spain	Ft. Huachuka, AZ, USA	Golden, CO, USA
Concentrator type	Glass mirror facets	Glass mirror facets	Stretched membrane	Stretched steel membrane, glass mirror tiles	Aluminized plastic film modules	Stretched membrane faceted glass mirrors
Concentrator aperture [m^2]	91	91	227	44	42	118
Receiver	Tubular direct irradiation	Tubular direct irradiation	Tubular direct irradiation	Tubular direct irradiation	Sodium heat pipe	Tubular direct irradiation /Hybrid
Engine	Kinematic Stirling	Kinematic Stirling	Kinematic Stirling	Kinematic Stirling	Kinematic Stirling	Kinematic Stirling
Electric output	25 kW_{el}	625 kW_{el}	53 kW_{el}	9 kW_{el}	7.5 kW_{el}	25 kW_{el}
Operation	1984-1985	1984-1988	1984-1988	1991-1998	1992-/	1995-/

Table 4.1.9. Dish farm projects.

	White Cliffs, Australia	Sulaibyah, Kuwait	Shenandoah, USA	Solarplant 1, USA
Rated power	25 kW_{el}	153 kW_{el}, 400 kW_{th}	400 kW_{el}, 2000 kW_{th}	4920 kW_{el}
Number of dishes	14	56	114	700
Concentrator type	Glass mirror facets	Glass mirror facets	Polymer film	Polymer film
Concentrator aperture [m^2]	227	1025	4332	30590
Heat transfer fluid	Water	Synthetic oil	Synthetic oil	Water
Engine	Steam	ORC	Steam turbine	Steam turbine
Storage	Lead acid battery	700 kWh thermal	1600 kWh thermal	no
Operation	1982-/	1984-/	1985-/	1985-1990

4.1.7.5 Central receiver power plant

A different approach for three-dimensional concentration on a larger scale is the central receiver or solar tower concept. Figure 4.1.40 shows the schematic of a tower plant. Two-axis tracking and concentrating mirrors, the heliostats, reflect the sunlight onto a single receiver located on top of a tower. The annual energy yield can be improved if the heliostat field surrounds the tower. Higher solstice efficiency can be achieved with the North field configuration (North field on the northern hemisphere, South field on the southern hemisphere). The spacing and size of the individual heliostats must be optimized with respect to land use, shadowing between the heliostats, tower height and several other parameters [91Win]. The single heliostat should have a size of the order of 25-150 m². Several hundreds up to thousands of heliostats are needed in a multi-megawatt plant. The tower height was in the range of about 50-100 m for the realized prototype plants having a power output of 1-10 MW_{el}, and will be of the order of 150-200 m for a 100-150 MW_{el} plant. Table 4.1.10 shows the data of the main central receiver projects discussed in

[95Bec], [93Bec], [91Win], [00Rei], [94Sol]. All the projects are terminated and larger plant designs are based on studies (e.g. a 30 MW air cooled tower plant in [88Pho], [90Pho]).

The collected solar energy is delivered to a heat transfer medium in the receiver. Different materials have been investigated as candidates for a tower heat transfer medium:

- Water/steam;
- Thermo oil;
- Molten salt;
- Liquid metals (e.g. sodium);
- Air.

Except air the media were tested in prototype plants (see Table 4.1.10). Thermo oil is not stable for temperatures above 300-400°C. This implies that the high temperature potential of the point focusing tower design cannot be exploited when using oil. Molten salt has the advantage not to need pressurization at higher temperatures. It can therefore directly be used as heat storage medium. The most recent prototype plant was the 10 MW_{el} Solar Two project in California [00Rei]. A photograph of this plant is shown in Fig. 4.1.41 where the surrounding heliostat field and the tower with the receiver can be seen.

Liquid metals like sodium have a high potential with respect to heat conductivity and heat capacity. But its high inflammability and connected safety aspects enforce many precautions when designing the hydraulic circuits. In the SSPS CRS tower plant liquid sodium was used as heat transfer fluid. It has the advantage of allowing high flux density receivers because of the good thermodynamic material properties. Besides this, it also served as heat storage medium in a two tank system. A sodium fire accident at the SSPS central receiver facility showed the necessary care in handling this fluid.

Air as heat transfer fluid is a good candidate with respect to environmental safety aspects and temperature resistance, but its density and thermal storage capacity is poor. A 2.5 MW volumetric air receiver was developed and tested at the Plataforma Solar de Almeria in Spain [94Hae]. The potential of the air technology could successfully be demonstrated.

Table 4.1.10. Solar central receiver plants.

Name	Location	Operation	El. output [MW]	Heat transfer fluid	Storage	Heliostat field aperture [m²]	Tower height [m]
SSPS	Almeria, Spain	1981-1986	0.5	Liquid sodium	Sodium, 2 h	3655	43
EURELIOS	Adrano, Italy	1981-1984	1	Steam	Salt/Water, 0.5 h	6216	55
Sunshine	Nio Town, Japan	1981-1986	1	Steam	Hitec salt [1]), 3 h	12912	69
CESA 1	Almeria, Spain	1983-1984	1	Steam	Hitec salt [1]), 3.5 h	11880	60
THEMIS	Targasonne, France	1982-1986	2-2.5	Molten salt	Hitec salt [1]), 5 h	10794	106
Solar One	Barstow, CA, USA	1982-1988	10	Steam	Oil/Rock, 3 h	71447	90
SES-5	Shchelkino, Russia	1985-?	5	Steam	0.3 h	40584	80
Solar Two	Barstow, CA, USA	1996-1999	10	Molten salt	Molten salt, 3 h	81400	90

[1]) Hitec salt: Mixture of KNO_3, $NaNO_2$, $NaNO_3$, melting at 140-220°C.

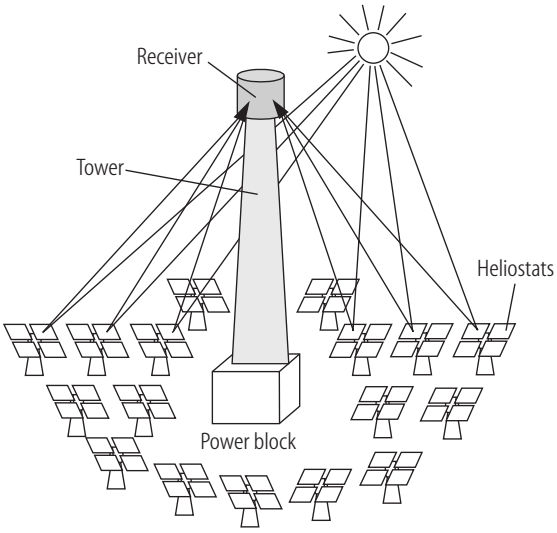

Fig. 4.1.40. Principle of a solar thermal tower plant. An array of heliostats concentrates light onto a receiver located on top of a tower.

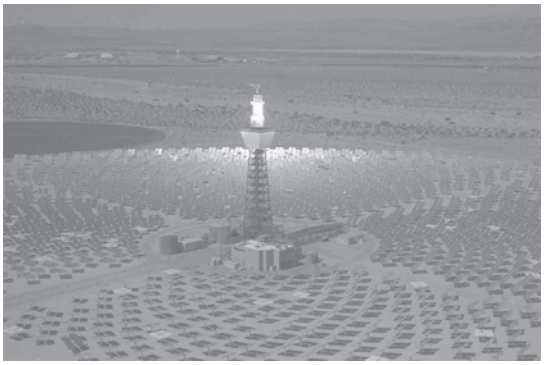

Fig. 4.1.41. Solar Two power tower plant. The surrounding heliostat field illuminates the molten salt receiver on the top of the tower (courtesy of Southern California Edison).

4.1.8 Comparison of solar thermal power plants

The following pages show comparisons of the different solar thermal power plant concepts. As many of the performed projects were prototype plants or test devices the given data have to be handled with the appropriate care.

4.1.8.1 Performance

Table 4.1.11 shows characteristic peak efficiency, average annual efficiency and capacity factor for the discussed solar thermal plant concepts. As in the field of solar thermal power production only a few plants were built for each of the technologies, the given figures correspond to prototype data or extrapolated performances. It is not possible to find statistically significant numbers.

The efficiencies of pond and chimney technology are very low, but the advantage of having natural storage media (water, soil) as a part of the system makes higher capacity factors possible. The direct Sun-tracking dish coupled to a Stirling engine gave the highest measured conversion efficiency from solar to electric of about 30%. The dish also has the lowest direct irradiance threshold for operation startup.

Table 4.1.11. Main operational characteristics of solar thermal plants.

System	Peak efficiency	Annual efficiency	Annual capacity factor
Pond	-	< 1%	Depending on pond size
Chimney	1% (Manzanares)	0.5% (Manzanares)	10% (Manzanares)
Trough	20% (SEGS)	10-12 %	24 % (no storage)
Tower	23% (projected)	14-19 %	25% (70-90% with storage)
Dish	29% (MDAC)	18-23 %	25% (no storage)

The annual capacity factors can be increased by implementing a storage system. The thermal storage efficiency increases with its mass, which means that such a system is best suited for large scale plant concepts like trough or tower. Furthermore, the tower has the advantage of delivering the energy on a higher temperature level, which is also favorable for efficient usage of the storage material.

4.1.8.2 Costs

In order to have an idea of the installation and electricity costs for the various solar thermal power plant technologies, a cost breakdown for the installations will be shown. No data were available for the solar pond because the costs strongly depend on geographical and geological conditions. For the chimney, trough, dish and tower technology the cost breakdown can be estimated (see Table 4.1.12). In any of these technologies the collector amounts to 40-50% of the total plant costs. Therefore, it is a high priority to optimize the collector technology. On the other hand increasing the cycle efficiency will reduce the area of the collector for a given electric output and contribute to a more economic plant.

Installation costs in US$/kW as well as the levelized electricity costs in US$/kWh are compared in Table 4.1.13. At the actual technological state (year 2002) the solar thermal power amounts to about 3000-10000 US$/kW installed, and a future market driven cost reduction could bring costs down to very attractive levels. The stated electricity costs for the trough technology of 0.12 US$/kWh (1998) are the result of a permanent optimization and increased routine in plant operation gained over many years of power production [98Cab].

Figure 4.1.42 shows a comparative plot of electricity production costs for the solar technologies compared to conventional plants. The conventional path is based on diesel generators for the small-scale power blocks and oil/coal for large-scale energy conversion plants.

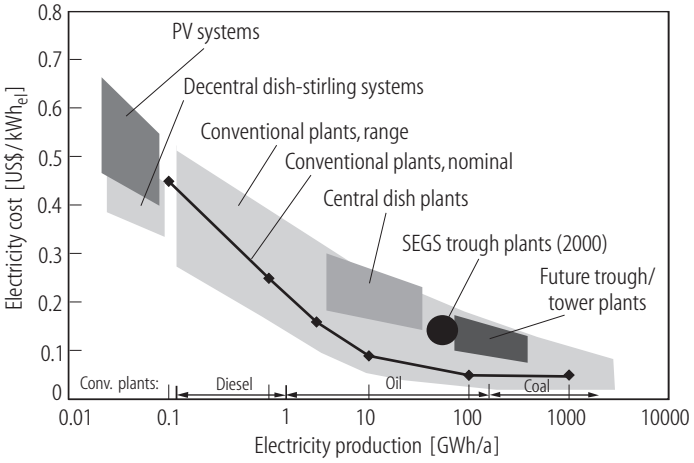

Fig. 4.1.42. Overview of electricity production costs.

Table 4.1.12. Cost breakdown for solar thermal power plants (chimney system costs come from a projected 5 MW plant, [00Sch]).

	Trough [%]	Dish [%]	Tower [%]	Chimney [%]
Collector	48	48 (including control)	37	40
HTF system	10		12 (Receiver)	31 (Chimney)
Power block	18	28 (Stirling engine)	26	17 (Turbine & Generator)
Infrastructure	3	2	2	5
Others	21	23	23	7
Total	100	100	100	100

Table 4.1.13. Estimated costs for solar thermal plants.

System	$/kW$_{el}$	$/kWh$_{el}$
Trough	4500 - 2900 (SEGS I-VII)	0.12 (actual, SEGS plants)
Tower	10000 - 3000	0.1 - 0.3 (studys, US and Phoebus)
Dish	20000 - 4000	0.4
Pond	3000 - 5000	0.3 - 0.6 [94Sol]
Chimney	5000	0.1 - 0.4 (100 MW 3rd Generation Plant, [00Sch])

4.1.9 Outlook

The technology and feasibility of solar thermal energy conversion and power production has been successfully demonstrated in several projects using dishes, troughs and towers, ranging from kilowatts up to more than 50 megawatts per unit. Looking at future potential, it can be stated that the electricity production costs will drop and may be competitive to conventional power plant technology, assuming the use of optimized and low-cost heliostats (cheap mirror technology, e.g. stretched membranes or thin glass on polymers), high temperature receiver and storage systems and locations with high direct normal irradiance in the Sun belt.

After having built more pilot plants in the 10-30 MW class and larger plants consisting of modules with several hundreds of MW each, energy production costs of less than 0.10 US$ per kWh_{el} may be attainable within a few decades. The energy may be delivered to all continents and consumers by large-scale power grid networks, preferably based on high voltage DC current transmission.

4.1.10 References for 4.1

53Kui Kuiper, G.P.: The Sun; The University of Chicago Press, 1953.

69Kon Kondratyev, K.YA.: Radiation in the atmosphere, New York: Academic Press, 1969.

75Gre Grether, D., Nelson, J., Wahlig, M.: Measurement of circumsolar radiation, Progress Report, Lawrence Berkeley Laboratory, 1975.

79Big Biggs, F., Vittitoe, C.N.: The helios model for the optical behaviour of reflecting solar concentrators, Sandia Report SAND 76-0347, 1979.

81Har Harris, J.A., Duff, W.S.: Focal plane flux distributions produced by solar concentrating reflectors; Solar Energy **27** (5) (1981) 403.

83Iqb Igbal, M: An introduction to solar radiation, Toronto, Canada: Academic Press, 1983.

87Joh Johansson, L.: Daily performance data of the McDonnell Douglas Dish Stirling Module, Technical Report, Louisville/KY: Phoenix Holdings Inc., 1987.

87Sch W.Schiel, M.Geyer, R.Carmona, The IEA/SSPS High Flux Experiment, Berlin: Springer-Verlag, 1987 (ISBN 3-540-18224-1).

88Kne Kneizys, F.X., Shettle, E.P., Abreu, L.W. et al.: User Guide to LOWTRAN 7; Air Force Geophysics Laboratory, Project 7670, Hanscom AFB, MA 01731 (AFGL-TR-88-0177 Environmental Research Papers, No.1010), 1988.

88Ney Ney, E.J.: The Shenandoah solar total energy project overview and operational experiences, in: American Solar Energy Society (ed.): Proceedings of the 1988 Annual Meeting of the American Solar Energy Society, Cambridge, June 20-24, 1988.

88Pho Phoebus Consortium: International 30 MWel Solar Power Plant, Phase 1A, Executive Summary, 1988.

88Wil Williams, T.A., Dirks, J.A., Brown, D.R., Antoniak, Z.I., Alleman, R.T., Coomes, E.P., Craig, S.N., Drost, M.K., Humphreys, K.K., Nomura, K.K.: Solar thermal bowl concepts and economic comparisons for electricity generation, Technical Report PNL-6129, Richland/WA: Battelle National Laboratories, 1988.

89Kas Kasten, F., Young, A.T.: Revised optical air mass tables and approximation formula; Appl. Opt. **28** (1989) 4735-4738.

89Wel Welford, W.T., Winston, R.: High collection non-imaging optics, New York: Acad. Press, 1989.

90Pho Phoebus Consortium: A 30 MWel Solar Power Plant for Jordan, Phase 1C, Feasibility Study, 1990.

91Bec Becker, M., Funken, K.-H., Schneider, G. (eds.): Solar thermal energy utilization, Berlin, Heidelberg: Springer-Verlag, 1991 (ISBN-3-540-53269-2).

91Din Dinter, F., Geyer, M., Tamme, R. (eds.): Thermal energy storage for commercial applications; a feasibility study on economic storage systems, Berlin: Springer Publ. House, 1991.

91Kan Kaneff, S.: Viable arrays of large paraboloidal dish solar thermal collectors, in: American Solar Energy Society (ed.): Proceedings of the Biennial Congress of International Solar Energy Society, Solar World Congress, Denver, 1991.

91Kes Kessler, S.: DIDIER Mixed Tube/Volumetric Receiver, in: Proceedings of the Volumetric Receiver Workshop, Köln, Böhmer, M., Meinecke, W. (eds.), DLR Techn. Report 2/91, 1991.

91Win Winter, C.-J., Sizmann, R.L., Vant-HullL, L.: Solar Power Plants, Berlin, New York: Springer-Verlag, 1991 (ISBN 0-387-18897-5).

92Kal Kalina Cycle Tested at Canoga Park. Modern Power Systems (MPS), March 1992.

93Bec Becker, M., Klimas, P. (eds.): Second generation central receiver technologies: A status report, Karlsruhe: C.F. Müller Publishing Co., 1993.

94Hae Haeger, M., Keller, L., Monterreal, R., Valverde, A.: Phoebus Technology Program Solar Air Receiver (TSA). Report Nr. PSA-TR02/94, Plataforma Solar de Almería, 1994.

94Sol Solar thermal electricity: A technology survey, status and trends, Sydney, Australia: Pacific Power, 1994 (ISBN 0-646-11271-6).

95Bec Becker, M., Gupta, B., Meinecke, W., Bohn, M. (eds.): Solar energy concentrating systems, Heidelberg: C.F. Müller, 1995 (ISBN 3-7880-7483-3).

98Cab Cable, R.G., Cohen, G.E., Kearney, D.W, Price, H.W.: SEGS Plant Performance 1989-1997, Proceedings of the International Solar Energy Conference Solar Engineering 1998, ASME Albuquerque, 1998 (ISBN No. 0-7918-1856-X).

98Neu Neumann, A., von der Au, B., Heller, P.: Measurement of circumsolar radiation at the Plataforma Solar (Spain) and at DLR (Germany), Proceedings of the International Solar Energy Conference Solar Engineering 1998, ASME Albuquerque, 1998 (ISBN No. 0-7918-1856-X).

99Neu Neumann, A., Witzke, A.: The influence of sunshape on the DLR solar furnace beam; Solar Energy, **66** (6) (1999) 447 - 457.

00Rei Reilly, H.E., Pacheco, J.E.: Solar Two: A successful power tower demonstration project, ASME Proceedings Madison, WI, 2000.

00Sch Schlaich, J., Schiel, W.: Solar chimneys, in: Encyclopedia of Physical Science and Technology, Third Edition, 2000.

03Hof German Patent No. 10149806.3-15, 13.11.2003.